REVIEW

Check for updates

Advances in catalyst and reactor design for methanol steam reforming and PEMFC applications

Eleana Harkou,†[a] Hui Wang,†[bc] George Manos, [ID][c] Achilleas Constantinou [ID] *[a] and Junwang Tang [ID] *[cde]

Hydrogen (H_2) is a clean energy carrier with significant potential for power and heat generation, offering a pathway to reduce emissions from fossil fuels. Over the years, various feedstocks have been explored for H_2 production, addressing the storage challenges associated with hydrogen. Methanol (MeOH) has emerged as one of the most efficient hydrogen storage medium. Among the different MeOH conversion processes, steam reforming stands out for its high hydrogen selectivity. This review focuses on recent catalyst development, in particular MSR reactor design and configuration, an area that has received comparatively limited attention in previous studies. Innovative reactor configurations, such as membrane and small-scale reactors, address the limitations of traditional packed-bed units, including pressure drop, heat and mass transfer resistances, and scalability challenges. By systematically analysing various reactor configurations, we address a critical gap in existing reviews and deliver innovative strategies for process optimisation. Additionally, the integration of methanol steam reforming with fuel cell systems presents a promising solution for reducing emissions in the transport sector. The review also discusses the relevant understanding on reaction mechanisms involved, followed by both the challenges and future prospects, emphasizing the importance of evaluating not only the environmental impact of these emerging technologies but also their manufacturing and operational costs.

[a]*Department of Chemical Engineering, Cyprus University of Technology, 57 Corner of Athinon and Anexartisias, 3036 Limassol, Cyprus. E-mail: a.konstantinou@cut.ac.cy*

[b]*College of Environmental Science and Engineering, Hunan University, Changsha 410082, P. R. China*

[c]*Department of Chemical Engineering, University College London (UCL), WC1E 7JE, London, UK*

[d]*Industrial Catalysis Centre, Department of Chemical Engineering, Tsinghua University, Beijing 100084, China. E-mail: jwtang@tsinghua.edu.cn*

[e]*Ordos Laboratory, Inner Mongolia, 017000, China*

† These authors contributed equally to this article.

Ms Eleana Harkou is a PhD candidate at Cyprus University of Technology, with a background in Chemical Engineering. She is skilled in both Computational Fluid Dynamics (CFD) simulations and process modeling, with extensive experience in the modeling, development, and scaling of chemical reactors for diverse applications and in optimising fluid flow, heat/mass transfer, and chemical processes. She specialises in

Eleana Harkou

the reaction engineering field with main focus on the reactor design to maximise the efficiency and performance of catalytical reaction processes.

Dr Hui Wang is a professor at the College of Environmental Science and Engineering, Hunan University. She received her PhD in Chemical Engineering from University College London under the supervision of Prof. Junwang Tang. Her current research focuses on photo-thermo catalysis for hydrogen production from biomass molecules, as well as the high-value transformation of pollutants.

Hui Wang

1. Introduction

The escalating environmental crisis, driven primarily by human activities and the extensive exploitation of fossil fuels for transportation, energy, and industrial purposes, necessitates urgent transitions to sustainable energy solutions. Hydrogen (H_2) has emerged as one of the most promising alternatives, offering a clean energy carrier capable of replacing fossil fuels through its conversion into power or heat.[1] The application of H_2 in fuel cell technology demonstrates comparable performance to traditional fossil-fuel-based systems, making it an attractive option for various applications, including vehicles

and heating systems. However, challenges related to its production cost, storage and transportation, persist, hindering the widespread adoption of H_2 technologies.[2]

Integrating H_2 into energy strategies is both crucial and necessary, particularly in the context of decarbonization efforts within the transportation and industrial sectors.[3] One of the primary challenges associated with H_2 is its low volumetric energy density, which complicates storage and increases costs. To address these issues, various storage methods have been explored, including liquid hydrogen, compressed hydrogen, and chemical storage using materials such as ammonia, metal hydrates, synthetic hydrocarbons, carbohydrates, formic acid, and liquid organic hydrogen carriers (LOHCs).[4,5] Among these, methanol (MeOH) has garnered significant attention as an effective liquid H_2 carrier due to its high H_2 conversion efficiency.[6] MeOH is a preferred H_2 carrier as it also has the same H/C ratio as methane and is a liquid under standard environmental conditions. Additionally, its conversion to H_2 occurs at lower temperatures, requiring less energy than fuels with C–C bonds, and it produces lower levels of CO due to milder operating conditions.[7]

Methanol Steam Reforming (MSR) stands out as a mature and economically feasible technology for H_2 production. Industrially, MeOH is converted to H_2 through reforming, with steam reforming being the most established process. Among the various reforming methods—MSR, methanol partial oxidation (POX), and methanol autothermal reforming (ATR), MSR is preferred due to its better H_2 to CO ratio.[8] Furthermore, other H_2 carriers such as formic acid, ammonia and hydrous hydrazine also show significant promise. Formic acid can be decomposed into H_2 under mild conditions.[9] In this liquid organic hydrogen carrier (LOHC) system, CO_2 is utilized in the

Dr George Manos is an Associate Professor of Chemical Engineering at University College London (UCL). His research involves hydrocarbon reaction processes with a focus on plastic waste catalytic pyrolysis and more generally catalysis on renewable energy processes. He is also working on catalyst deactivation by coking and coke characterisation, as well as statistical mechanical modelling of adsorption on microporous materials.

George Manos

Dr Manos is the author of more than one hundred refereed journal papers, as well as numerous book chapters and conference papers. He is the co-editor of the book Adsorption and Phase Behaviour in Nanochannels and Nanotubes.

Dr Achilleas Konstantinou is an Assistant Professor at Cyprus University of Technology (CUT). He specializes in Chemical and Catalytic Reaction Engineering, and in particular in designing multiphase reactors to intensify and improve their performance for industrial applications. Dr Konstantinou has made extensive use of complex Computational Fluid Dynamics (CFD) tools and successfully validated the prediction of concentrations,

Achilleas Constantinou

temperatures and velocity profiles in micro-units against experimental findings, in order to improve their design and render them suitable for industrial production. Dr Konstantinou also holds the titles of Chartered Chemical Engineer (MIChemE), Chartered Engineer (CEng) and Chartered Scientist (CSci).

Prof. Junwang Tang is a Member of Academia Europaea, a Leverhulme Trust Senior Research Fellow, a Fellow of RSC, a Fellow of European Academy of Sciences and formerly a full Professor at the Department of Chemical Engineering in University College London. He is currently a Chair Professor of Materials Chemistry and Catalysis in the Department of Chemical Engineering and Director of the Industrial Catalysis

Junwang Tang

ysis Centre at Tsinghua University. He has concentrated on photocatalysis and has pioneered in photon–phonon co-driven catalysis for the activation of small molecules (e.g., H_2O, CO_2, CH_4 and N_2) as well as microwave catalytic depolymerisation of plastics. He has received many prestigious honors, including the 2022 IChemE Oil and Gas Award, the 2021 IChemE Andrew Medal, the 2021 RSC Corday-Morgan Prize, and the 2021 IChemE Innovative Product Award.

formation of formic acid, making it a safer and more convenient H_2 carrier to handle.[10] Ammonia is also regarded as an excellent H_2 carrier molecule as it possesses a high H_2 content of around 18 wt% and a large energy density of up to 3000 W h kg^{-1}. Hydrous hydrazine, with a high H_2 content of 8 wt%, can also be decomposed to produce H_2 and nitrogen (N_2) by a carbon-free process. However, an undesired side reaction can generate ammonia, which affects the selectivity towards H_2 and the overall efficiency of the process.[11,12]

Despite the extensive research on catalyst development for methanol reforming, the studies have primarily concentrated on catalyst-related aspects, with less attention given to innovative reactor technologies and whole chemical processes.[8,13–19] This review aims to fill this gap by providing an up-to-date overview of various reactor units used in MSR, detailing their operational parameters and highlighting the benefits of membrane and microreactor systems besides a discussion on new catalyst development and mechanistic results. Additionally, this review examines the integration of the MSR reaction with Proton Exchange Membrane Fuel Cells (PEMFCs), extending beyond catalyst-related topics to include mechanistic insights.

2. Thermostatic materials

Due to the rise of environmental issues, the evaluation of existing energy processes and operations is a crucial factor concerning the research community. Among the products of the reaction, small amounts of CO are required for PEMFC applications. Emphasis should be placed on catalyst design to achieve high selectivity toward H_2, making the produced CO negligible.[13] The two side reactions that occur during the MSR are the MeOH decomposition and the water gas shift (WGS) reaction, which occurs when the steam/MeOH ratio is low. In contrast to MeOH POX, MSR is an endothermic reaction that yields high H_2 and is widely preferred.[14]

In recent years, efforts have been made to improve the performance of conventional catalysts regarding the MSR reaction since Cu-based catalysts suffer from poor stability, sintering and carbon deposition, with the latter two being the most frequent issues. Improving preparation methods, adding promoters and optimising support materials could significantly enhance the stability of such catalysts.[20] Moreover, the introduction of nanoparticles or porous materials can further improve conventional catalysts.[21] Many catalysts have been suggested for H_2 production showing long-term stability under high temperature conditions over a suitable support. Table 1 summarises the key features regarding the investigated catalysts.

Noble metals, such as Rh and Pd, were found to be advantageous by achieving high H_2 yields and good stability, although their high cost hinders their application to different commercial systems.[33] Ni-based catalysts, due to their low cost, are preferred for the MSR reaction, and their combination with Cu can significantly reduce CO formation. In a recent study, a Ni–Cu/Al_2O_3 catalyst was investigated, showing that by increasing the Ni content and catalyst loading almost 100% MeOH conversion was achieved, but at the same time the increase of the Ni content enhanced the MSR performance and RWGS reaction leading to higher CO concentrations.[22]

Bimetallic Ni–Cu catalysts supported on ZrO_2 were examined by Lytkina et al.,[23] with different ratios of nickel and copper and annealing temperature. Fig. 1 displays the H_2 yields of the investigated catalysts with temperature gradient. Maximum H_2 production was achieved at a lower annealing temperature (350 °C), where the sample was primarily represented by non-
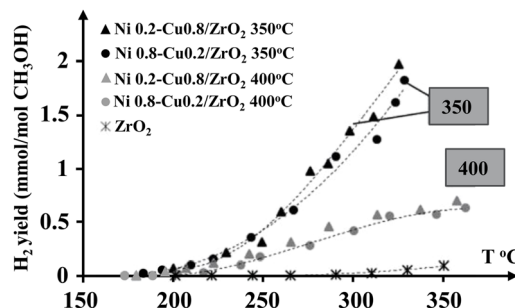

Fig. 1 H_2 yields of different ratios of Ni–Cu catalysts.[23] Reproduced from ref. 23 with permission from Elsevier, Copyright 2015.

Table 1 Thermostatic materials investigated for MSR

Catalyst	Pressure (bar)	Temperature (°C)	S/C ratio	MeOH conversion (%)	CO selectivity (%)	H_2 selectivity (%)	H_2 yield (mol/mol$_{MeOH}$)	Ref.
10% Ni–Cu/Al_2O_3	—	250	2	100.0		—	2.66	22
$Ni_{0.2}$–$Cu_{0.8}/ZrO_2$	1	325	—	—		—	2.00	23
Cu–Ni/TiO_2/monolith	1	300	2	92.6	9.6	92.7	—	24
$CuZrAl_{0.4}$	1	270	1.5	96.0		—	—	25
CuZnZrAl(Co–Am)	1	270	1.2	100.0	0.3	—	—	26
ZrO_2-0.1/Cu	1	300	1	90.0	—	—	—	27
Cu/ZnO/Al_2O_3–5Mg	1	200	1	68.0	—	—	—	28
CuCe–MC (IMP)	—	250	3	68.0	17.0	>95.0	—	29
5% Cu/CeO_2	—	340	—	76.0	1.1	—	—	30
5% Cu/Sm_2O_3	—	340	—	76.0	0.9	—	—	30
2% Pt/α-MoC	60	190	—	—	<0.1	—	—	31
15Pt/15In_2O_3/CeO_2	1	350	1.4	99.9	2.9	74	—	32

crystallised mass. MeOH-involved H_2 production hardly occurred on pure Zr. Conversely, with calcined catalysts at 350 °C, a higher H_2 yield could be obtained. However, the most active samples were the ones where the tetragonal ZrO_2 was coated with an amorphous shell. Also, the conversion of MeOH on Cu-rich catalysts was more selective in the H_2 production. The difference between the Cu-rich and Ni-rich catalysts in selectivity was due to the character of the predominant metal, showing itself in a change of Fermi level, as well as in chemical properties.

Tahay et al.[24] studied the MeOH-involved H_2 production process utilising a micro-structured monolith in conjunction with a synthesised nanostructure of TiO_2. The surface of the monolith/TiO_2 was coated with Cu, Cu/Ni, Ru and Pt metals. The monolith structure significantly improved the mass transfer of reactants and products, and, in synergy with the high surface area, porosity, pore size, and stability of the nanostructured TiO_2 film, the MeOH conversion was found to reach 99% with low CO selectivity (5%). Among the investigated catalysts, the Ru catalyst exhibited the highest conversion and selectivity. However, due to economic considerations, the Cu–Ni catalyst presents an excellent alternative, achieving a 93% conversion rate. Furthermore, similar to previous studies, the MeOH conversion and H_2 selectivity of the Cu–Ni catalyst were superior to those of the pure Cu catalyst, attributed to the role of Ni.

The primary challenge with commercial catalysts is deactivation, where various cocatalysts or promoters play a crucial role in enhancing the reforming stability and activity.[34] For example, acidic or alkaline cocatalysts can further convert undesired products into valuable or less harmful ones, thereby improving the catalytic performance. Although highly dispersed Cu-based catalysts have been reported to achieve high activity with reduced CO formation, there is no consensus on the promotion mechanism.[35,36] Moreover, the inclusion of a second promoter, along with diverse supports, may influence both activity and selectivity. There has been sustained interest in supports and promoters, with certain materials, such as ZnO, CeO_2, Al_2O_3 and ZrO_2, showing dual functionality by improving catalyst activity and stability through modifications in dispersion and interactions with the support material.[37] It is widely recognized that isolated metal atoms exhibit exceptional performance in various reaction systems. However, the absence of ensemble sites limits their ability to facilitate the reaction of large molecules and certain multistep processes. Consequently, the "ensemble effects" between single metal atoms and neighbouring oxygen vacancies can enhance and promote the catalytic activity for reactions involving large molecules.[38] The catalytic activity of Cu-based catalysts has been found to improve with both ZrO_2 and ZnO promoters, which could enhance the surface area, stabilise Cu crystal size, prevent agglomeration of Cu particles during reduction and reaction processes, and stabilise Cu^+ species on the catalyst surface.[39] For instance, Pd/ZrO_2 provided the best activity for H_2 generation, but Pd/ZnO gives a high CO_2 selectivity (97%).[40] Different synthesis approaches impart distinct properties to catalytic materials. For instance, the sol–gel auto-combustion method

used in the synthesis of Cu/ZrO_2 catalysts has been found to achieve higher CO_2 selectivity, activity, and stability compared to catalysts prepared through impregnation and co-precipitation methods.[41]

Mateos-Pedrero et al.[25] investigated the performance of a newly synthesised catalyst, Cu over a ZrAl support. The new catalyst aims to improve the catalytic performance and promote non-CO generation. The major drawbacks of the most conventional Cu-based catalysts are the absence of lifelong stability and hence the activity loss and the formation of CO. The investigation showed that the composition of the support has a huge effect not only on the catalyst performance but also on the physicochemical characteristics of the CuZrAl catalyst. Moreover, the inclusion of zirconia and its content in the supported catalyst yielded interesting results. A high zirconia content led to lower activity due to zirconia segregation, as Zr has a low surface area. Conversely, at a low zirconia content, ZrAl samples exhibited a homogeneous composition with high dispersion of Zr and Al species. This improved dispersion and reducibility of the catalyst proved advantageous for catalytic performance.

Li et al.[26] synthesised different CuZnZrAl catalysts via the coprecipitation-ammonia method as well as investigated the influence of Y and Ce promoters. The results revealed that this preparation method enhanced the dispersion of each component in the catalyst, leading to smaller crystal sizes and larger surface areas. The addition of promoters, particularly Ce, improved the catalyst's stability, achieving 100% conversion at 270 °C with a CO selectivity of just 0.3%. Furthermore, after 20 cycles, the conversion remained as high as 98%.

Xu et al.[27] developed an inverse ZrO_2/Cu catalyst through an oxalate sol–gel co-precipitation followed by calcination/H_2-reduction treatment. The catalyst consisted of highly dispersed t-ZrO_2 nanofragments with size between 3 and 4 nm over the Cu substrate with particles of around 20 nm size. The inverse catalyst showed exceptional stability in terms of long-term catalytic performance with zero CO production and a high yield of 190 $mmol_{H_2}$ g_{cat}^{-1} h^{-1} at 200 °C. Both DFT calculations and experimental results demonstrated that the highly reactive interface of –OH groups resulting from the formation of a ZrO(OH)–(Cu^+/Cu) interfacial structure during the reaction can convert HCHO* to H_2 and CO_2 with HCOOH* as an intermediate.

Cheng et al.[28] used the base of an industrial Cu/ZnO/Al_2O_3 catalyst to enhance the Cu–ZnO synergy. CuZnAl–xMg catalysts were synthesised with different Mg loadings, and the addition of a Mg dopant was found to promote the catalytic activity, reaching the greatest space time yield of H_2 of 172 mmol g^{-1} h^{-1} at 5% Mg content, attributed to the high surface area of Cu and abundant Cu^+ species. Characterisation techniques revealed a decrease in the particle size and an increase in the surface area with higher Mg loadings. XRD patterns indicated that up to 5% Mg, the crystal size of ZnO and Cu was reduced, enhancing the catalytic performance. However, when the Mg composition was increased to 7%, the crystal size of ZnO and Cu enlarged, suggesting that the positive effect of Mg may be weakened in the presence of excess Mg.

Li *et al.*[42] aimed to expose a commercial Cu/ZnO/Al$_2$O$_3$ catalyst to a mixture of H$_2$, H$_2$O, and CH$_3$OH at atmospheric pressure and 300 °C to accelerate the migration of ZnO$_x$ species onto the surface of Cu metal through an adsorbate-induced strong metal–support interaction. The results demonstrated that such morphological modifications could enhance the stability by approximately 70%. Moreover, the catalytic activity was improved, and the MSR reaction was promoted.

The influence of Ce and Zn on a Cu-based mesoporous carbon (MC) catalyst was studied by Bepari *et al.*[29] These catalysts are widely used for their large pore volume, well-structured porosity, and chemical inertness. The addition of Cu to the MC increased the pore volume due to the formation of Cu nanoparticles on the support surface, while the addition of Zn and Ce further increased the pore diameter in nearly all catalysts. Catalytic testing, conducted between 200 and 350 °C using a wet impregnation method for CuCe on MC, demonstrated the best conversion rate among the catalysts, achieving 68% at 250 °C. In terms of conversion, the addition of Ce using both the one-pot and wet impregnation methods resulted in higher performance compared to CuZn on MC prepared by the one-pot method. H$_2$ selectivity was high (>90%) for all catalysts, and the addition of Ce effectively inhibited carbon deposition.

Liu *et al.* made an attempt to synthesise more feasible catalysts and for the first time investigated Cu-based catalysts on different supports, including La$_2$O$_3$, Pr$_6$O$_{11}$, Sm$_2$O$_3$, Y$_2$O$_3$ and CeO$_2$.[30] Five different rare earth oxide (REO) supports were used to study the Cu/CuO–support interaction, revealing that the La$_2$O$_3$ support had a negative impact on the reaction, while all the other cubic-phase catalysts were successfully synthesised. Regarding MSR reaction performance, among the five synthesised catalysts, the 5% Cu/CeO$_2$ catalyst showed the best production performance, closely followed by the 5% Cu/Sm$_2$O$_3$ catalyst (Fig. 2). It was found that the quantities of surface basic sites, the active O$_2^-$ species, the Cu$^+$ content/percentage and the active Cu surface area positively affected the reaction performance. Moreover, the MeOH adsorbing/SR *in situ* DRIFTS results revealed that in the case of Cu/CeO$_2$ catalyst the m-HCOO* reactive monodentate intermediate was formed, while in the case of Cu/Y$_2$O$_3$ it was absent, making it the worst performing catalyst.

A Pd–Zn alloy was studied for thermocatalytic MeOH-involved H$_2$ production, and it was found that the catalyst underwent pre-reduction before the reaction would facilitate the catalyst activity. The mechanistic investigation revealed that
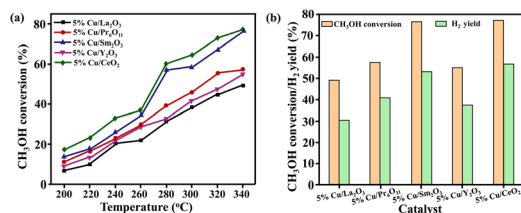
the formed HCHO underwent decomposition into CO and H$_2$ on metallic Pd, whereas HCHO present on the Pd–Zn alloy was transformed into CO$_2$ and H$_2$ through the interaction with H$_2$O.[43] Additionally, Ru was reported to enhance the activity of thermocatalytic methanol-involved H$_2$ production by promoting the dispersion of Pd particles. Characterisation results indicated that the promotion of CO desorption from Pd sites by Ru was the key factor for the observed activity enhancement.[44] Moreover, Au served as an efficient cocatalyst in CeO$_2$ catalysed MeOH-involved H$_2$ production at low temperatures (<250 °C), where strong bonded Au–O–Ce species were the main active species.[45] A single-atom system was also reported, in which Au and Pt were anchored on the lattice-O of ZnO.[46] Density functional theory (DFT) calculations suggested that the efficient catalysis of Pt$_1$ and Au$_1$ originated from the strong binding energy of the intermediates, reducing the reaction barrier height and maximising active atom utilisation.

Lin *et al.*[31] mentioned that Pt atomically dispersed on α-molybdenum carbide (α-MoC) enables low-temperature, base-free H$_2$ generation, with remarkable H$_2$ production activity in an aqueous phase system (Fig. 3a and b). Numerous studies have demonstrated H$_2$ generation through methanol-involved aqueous phase reforming over Pt- and Ru-based noble metal catalysts. The exceptional H$_2$ production was attributed to the strong ability of α-MoC to promote water dissociation and the synergistic effect between Pt and α-MoC, which effectively activated methanol and facilitated its reforming.

In a recent study of Lin *et al.*,[47] the MeOH-involved H$_2$ production was investigated using a newly discovered catalyst, Ni/α-MoC, where catalyst's production rate was 6 times greater than that of a conventional noble metal Pt/Al$_2$O$_3$ catalyst (Fig. 3c and d). The synergistic effect of CO reforming and C–H bond dissociation over the atomically dispersed Ni, as well as the
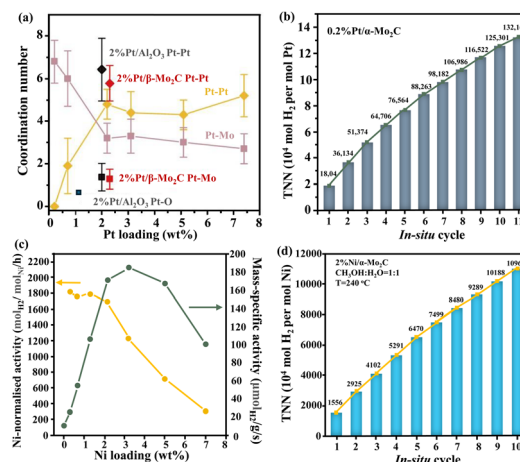
Fig. 3 (a) Coordination numbers as a function of Pt loadings in Pt/α-MoC catalysts. (b) MeOH-involved H$_2$ production activity on 0.2% Pt/α-MoC,[31] (c) average catalytic activity of Ni/α-MoC with different Ni loadings and (d) MeOH-involved H$_2$ production activity on 2% Ni/α-MoC.[47] TTN: total turnover number. (a) and (b) Reproduced from ref. 31 with permission from Spring Nature, Copyright 2017. (c) and (d) Reproduced from ref. 47 with permission from American Chemical Society, Copyright 2021.

Fig. 2 Catalytic MSR reaction tests. (a) MeOH conversion and (b) H$_2$ yield at 340 °C.[30] Reproduced from ref. 30 with permission from Elsevier, Copyright 2023 Elsevier Ltd. All rights reserved.

highly efficient O–H activation over α-MoC, were the main reasons for effective catalytic performance. The key factor for highly active Ni-based catalysts relies on the high surface area with adequate Ni dispersion along with the small particle size.[48]

Modragón-Galicia et al.[49] conducted a systematic investigation of the heterogeneous MSR reaction using three different catalytic materials: Pt/ZnO, Pd/ZnO, and PtPd/ZnO. X-ray diffraction (XRD) studies and profiles presenting crystallographic details revealed that the intermetallic PtZn phase on the Pt/ZnO catalyst was more stable compared to the PdZn phase on the Pd/ZnO catalyst. Additionally, platinum within the PtZn structure was found to be stabilized in the bimetallic PtPd/ZnO catalyst. Superior performance was demonstrated by measuring the catalytic reactivity of the Pt/ZnO-rod catalyst.

A Pt-based catalyst was investigated by Shanmugam et al.[32] on the MSR. The study examined the influence of various metal supports (CeO_2, Al_2O_3, and ZrO_2) and the presence of In_2O_3 as a co-support, which yielded significant results. The addition of the co-support facilitated the formation of metallic Pt nanoparticles with high concentration, improved dispersion, and controlled particle size on the surface. The activity and stability of these catalysts were enhanced, with a notable reduction in CO formation. Among the catalysts, the $Pt/In_2O_3/CeO_2$ catalyst exhibited excellent performance in MSR, demonstrating stability for 100 hours with the lowest CO formation. Additionally, single-atom Pt_1 deposited on CeO_2 offered significantly higher H_2 activity, which was 40 times greater than that of 2.5 nm Pt/CeO_2.[50]

Recently, low-temperature MeOH-involved H_2 production was reported,[51] where the synergy of Pt single atoms and Lewis pairs allowed porous CeO_2 to realise efficient H_2 generation at 120 °C, and a very low CO (0.027%) was observed. The catalyst design played a crucial role in the activation of both MeOH and H_2O, resulting in high H_2 production at lower temperatures – a challenging feat for single active-site catalysts. The construction of dual active-site catalysts suggests that a metal active site with high capability for methanol activation can exhibit low water dissociation, while water activation was promoted on reducible metal oxides through interaction with the O atom at a Lewis acidic centre, followed by transfer of one H atom to the adjacent Lewis basic centre. The $Pt_1/PN–CeO_2$ catalysts exhibited at 135 °C a H_2 generation rate of 199 mol_{H_2} mol_{Pt}^{-1} h^{-1}, which was a lot higher than those of Pt/Al_2O_3 (2.6 mol_{H_2} mol_{Pt}^{-1} h^{-1}), Pt/TiO_2 (3.8 mol_{H_2} mol_{Pt}^{-1} h^{-1}) and Pt/C (0.7 mol_{H_2} mol_{Pt}^{-1} h^{-1}) catalysts under the same conditions. The conventional metal-based catalysts utilised at the industrial level for the MSR reaction cannot operate at low temperatures such as 100–165 °C where the dual active site catalysts operate, since the temperature according to the Arrhenius expression

$$\left(k = A e^{\frac{-E_a}{RT}} \right)$$

is directly related to the reaction rate for H_2 production. The development of such materials not only improves the energy efficiency of industries but also contributes positively to addressing the environmental crisis.

Zhang et al.[52] conducted a morphological investigation evaluating different shapes of CeO_2, including rods (r), cubes (c), and irregular (w) forms, on a $Pd/In_2O_3/CeO_2$ catalyst prepared through the impregnation method. Catalytic performance results demonstrated that the $Pd/In_2O_3/CeO_2$-r catalyst exhibited the best performance, achieving nearly 96% methanol (MeOH) conversion at 375 °C. Although the primary products were H_2 and CO_2, minor amounts of CO, methane, and dimethyl ether were also detected. CO selectivity was approximately 1.3%, while the selectivity of other undesired products remained very low, at parts-per-million (ppm) levels. Scanning Electron Microscopy (SEM) and High-Resolution Transmission Electron Microscopy (HR-TEM) characterization revealed that the shape of the CeO_2 support affects the exposure of different crystalline surfaces, thereby influencing the catalytic activity. Specifically, in the rod-shaped morphology, the preferential exposure of the Ce (110) crystal facet provides abundant active Pd^0 species, active oxygen vacancies, and surface oxygen. These features assist in the activation of MeOH and H_2O during the catalytic cycle, thereby promoting the formation of CO_2 and H_2. Lastly, the stability of the $Pd/In_2O_3/CeO_2$-r catalyst was highlighted, along with its potential for utilization in PEMFC systems.

Thermocatalytic MSR is a widely used industrial technology for H_2 production, requiring high energy input due to the elevated operating temperatures. Efforts have been made to industrialise low-temperature MSR, attracting attention and finding applications in various areas. Research has primarily focused on catalyst development to improve the performance, selectivity, and stability. In addition to catalyst synthesis, other factors such as reactor design also influence the overall reaction performance and are discussed comprehensively below.

3. Reaction mechanism

The first attempt to explore the mechanism of surface reaction of different Cu-based catalysts was about three decades ago. The development of computational studies and hence the emphasis that has been given to the Cu-based surface reactions via DFT calculations are conducive to the better comprehension of the reaction mechanism while predicting catalyst surface pathways, reaction barriers and reaction energies for the MSR reaction.[53] There are extensive studies on the reaction kinetics of Cu catalysts as well as noble metal catalysts,[54-56] while recently we more often came across Ni-based catalyst investigations.

Bossola et al.[57] designed a Cu-based catalyst on zirconia with the addition of silica to zirconia in order to improve the electronic and morphological properties of the Cu nanoparticles. A sequence of characterisation techniques were performed to address the improved activity, with the suggested mechanism proposing that MeOH is adsorbed on Cu, which then goes through the dehydrogenation process via the formate pathway. The metallic part of the nanoparticles contributes to the H_2 production on the same site. Significant enhancement in the H_2 production was obtained for $Cu/ZrO_2–SiO_2$, which was four times greater than that of the silica-free catalyst.

Reyna-Alvarato et al.[58] theoretically studied the MSR reaction mechanism using different catalysts, such as CeO_2 and Ni/CeO_2, showing similar results as Zuo et al.[59] Their theoretical
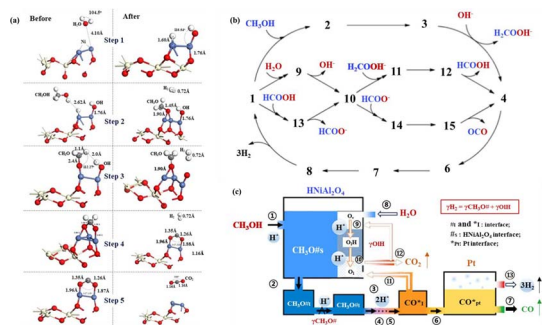
Fig. 4 (a) Schematic of the suggested theoretical catalytic mechanism of CeO_2 and Ni/CeO_2 in MeOH-involved H_2 production,[58] (b) the ruthenium-catalysed production mechanism of H_2 production from MeOH-involved H_2 production,[62] and (c) the overall process via Pt/$NiAl_2O_4$.[63] (a) Reproduced from ref. 58 with permission from Elsevier, Copyright 2021 Elsevier B.V. All rights reserved. (b) Reproduced from ref. 62 with permission from American Chemical Society, Copyright 2014. (c) Reproduced from ref. 63 with permission from American Chemical Society, Copyright 2023.

mechanism suggests that the reaction consists of 5 steps (Fig. 4a). Initially, the H_2O molecule is adsorbed over the catalyst surface which forms one hydroxyl group (OH) and one adsorbed hydrogen (H), and MeOH then reacts with the atomic H_2 forming a methoxy species ($-CH_3O$) at the catalytic surface. In the third step, another molecule of H_2 is released, forming one formaldehyde molecule ($-CH_2O$), which is considered as the intermediate reaction. The new formate is a result of the reaction between the H_2 molecule of the hydroxyl group and another H_2 molecule of the methoxy group. Consequently, a H_2 molecule is released with the subsequent decomposition of one formaldehyde molecule into H_2 and O–C, where the former is surface attached. Lastly, a third H_2 molecule and the remaining CO_2 molecule are released.

Fajin and Cordeiro[60] studied the MSR over Ni–Cu surfaces using DFT calculations to understand all the possible reaction routes, especially the ones achieving direct CO_2 formation from MeOH. The decomposition on the surface followed by the WGS reaction, which directly transformed the obtained CO to CO_2 and H_2, the direct conversion of MeOH into CO_2 and H_2 and possible methane and coke formation are the catalytic reaction routes that were considered in their work. The disruption of the O–H bond or one of the C–H bonds of MeOH starts its decomposition with further rupture of the remaining bonds to follow. The direct formation of CO_2 and H_2, is a pathway affiliated to the presence of combined phases in the catalyst. Formaldehyde can be obtained during the MeOH decomposition reaction with a co-adsorbed hydroxyl, and the attained compound (CH_2OOH) is converted on the surface until the generation of CO_2. Furthermore, the catalyst blocks the generation of methane or coke, while the desorption of CO is not to be expected.

A single Ni-embedded model (NiCu (111)) and a single Ni-adsorbed model (A-NiCu (111)) were developed by Tang et al.,[61] wherein DFT calculations were performed to assess their adsorption capacities and mechanistic investigation was

carried out. Both the considered bimetallic surfaces were found to have enhanced stability compared to the pure Cu (111), and the introduction of Ni also improved the adsorption performance. Additional investigations were conducted on adsorption enhancement, showing that the A-NiCu (111) surface has a stronger adsorption promoting effect. Regarding the reaction mechanism, three major procedures were taken into account during the MSR (MeOH dehydrogenation, water decomposition and RWGS reaction), while several intermediate reactions were considered indicating that the rate-determined step is the methoxy dehydrogenation. Moreover, the lower activation energy of the NiCu (111) surface during the CO conversion process plays a significant role in inhibiting coke deposition.

The reaction mechanism of MSR using Ru-based catalysts was investigated by Yang et al.,[62] wherein a DFT study was applied to reveal the catalytic cycles for the release of H_2 and CO_2. Three catalytic cycles participate in the reaction mechanism consisting of the MeOH to formaldehyde dehydrogenation, the formaldehyde coupling and the hydroxide to formic acid conversion as well as the formic acid dehydrogenation to CO_2. Fig. 4b shows the overall mechanism of the MSR reaction. The reaction begins with a hydroxyl proton transfer from a molecule of MeOH to the ligand N_2 of the catalyst and then the C–H bond splits with ease transferring the hydride to the metal centre of the catalyst for the formation of formaldehyde. The latter generates an anion that is a bit more stable with the hydroxide anion, which could be regarded as originating from the solvent or formed from the cleavage of H_2O. Then, the formation of formic acid through the disruption of a C–H bond happens for the transfer of a methylene hydride in the H_2COOH^- anion to Ru. Due to the acidity of formic acid, it is not possible to discover the transition state for the rupture of the O–H bond in formic acid. After every catalytic cycle, a molecule of H_2 is released through a self-promoted mechanism that features an extra MeOH or H_2O molecule acting as a bridge for the transfer of a proton from the ligand nitrogen to the metal hydride. Recently, steady-state isotopic transient kinetic analysis (SSITKA) was utilised to study the detailed process involving methoxyl and CO species adsorbed on Pt/$NiAl_2O_4$.[63] From Fig. 4c, C–H bond cleavage occurs within methoxyl adsorbed on interface sites, and O–H bond rupture is observed within oxygen-filled surface vacancies, respectively.

Xue et al.[64] aimed to investigate the gliding arc MSR (GA-MSR) reaction mechanism combining experimental data and plasma kinetic simulations at different MeOH concentrations. First, the H, OH and CH_3 were considered as the main reactive species as their concentrations increased due to their fast formation in the inside arc stage, while they were consumed up in the outside arc step during the thermochemical process. The main steps considered were the MeOH decomposition and dehydrogenation. The increase of MeOH concentration demonstrated an enhancement solely on the concentrations of H and CH_3, suggesting that at low MeOH concentrations CO_2 is produced and at higher MeOH concentrations hydrocarbons are produced.

Almithn and Alhulaybi[65] performed a mechanistic investigation using DFT calculations for Ni_2P. It was revealed that

Table 2 Reactor set-ups utilised for the MSR

Reactor	Design characteristics	Conditions	MeOH conversion (%)	H$_2$ yield (%)	Ref.
Continuous flow	Isothermal tubular packed bed reactor with an internal diameter of 1 mm and a length of 16 cm	230 °C, 0.86 bar, S/C = 1.1, and W/F = 35 kg$_s$ g^{-1} mol^{-1}	100.0	—	76
Continuous flow	Isothermal tubular coated wall reactor with an internal diameter of 4.1 mm and a length of 16 cm	230 °C, 0.86 bar, S/C = 1.1, and W/F = 40 kg$_s$ g^{-1} mol^{-1}	94.0	—	76
Continuous flow	Isothermal packed bed reactor with an internal diameter of 1.5 mm and a catalyst size of 150 μm	230 °C, 1 bar, S/C = 1.1, and m_{cat}/V_{in} = 2 [mg (μL^{-1} min^{-1})]	60.0	—	78
Continuous flow	Isothermal coated wall reactor with an internal diameter of 1.5 mm a and catalyst size of 150 μm	230 °C, 1 bar, S/C = 1.1, and m_{cat}/V_{in} = 2 [mg (μL^{-1} min^{-1})]	65.0	—	78
Continuous flow	Counter-flow tubular packed bed reactor with 8 internal heating tubes with an internal diameter of 12 mm and a length of 25 mm	T_{in} = 240 °C, 1 bar, and 8 heating tubes	94.5	61.7	79
Continuous flow	Tubular fixed-bed reactor with simultaneous internal and external heating	T_{in} = 250 °C, 1 bar, S/C = 1.5, and v = 0.2 m s^{-1}	100.0	62.8	80
Continuous flow	Non-isothermal multitubular packed bed reactor with a length of 0.5 m and thermal air passing through the shell side	$T_{thermal\ air}$ = 400 °C, T_{MeOH} = 160 °C, and 1 bar	95.0	65.0	82
Membrane	Packed bed reactor with Pd membrane for a H$_2$ purity of >99.99%	280 °C, 1 bar, S/C = 1.2, and Q = 1 g min^{-1}	97.0	91.1	83
Membrane	Fixed bed reactor with Pd membrane for a H$_2$ purity of >99%	280 °C, 1 bar, S/C = 1.2, and V = 0.5 mL min^{-1}	70.3	74.4	84
Membrane	Isothermal membrane reactor with a silica membrane (4 mm thickness and 5 cm active length)	300 °C, 1.5 bar, S/C = 1, and GHSV = 6000 h^{-1}	85.0	85.0	85
Membrane	Isothermal membrane reactor with a Pd–Ag membrane (50 μm thickness and 5 cm active length)	280 °C, 2 bar, S/C = 1, and GHSV = 1800 h^{-1}	100.0	100.0	85
Membrane	Isothermal membrane reactor with a silica membrane of 4 mm thickness	240 °C, 10 bar, S/C = 3, and GHSV = 6000 h^{-1}	95.0	96.0	86
Membrane	Non-isothermal membrane reactor with 4 membranes of 3 in. height and 1/8 in. diameter dead-end tubes coated with a 30 μm thick Pd–Ag active layer	450 °C, 6 bar, S/C = 1, and V = 0.02 mL min^{-1}	98.0	—	87
Membrane	Non-isothermal membrane reactor with a Pd–Ag membrane consisting of 600 ceramic support tubes	300 °C, 2 bar, S/C = 1, and sweep ratio = 1	94.0	93.8	88
Microreactor	Non-isothermal circle-triangle cross-sectional microreactor	T_{in} = 100 °C, 10 bar, and S/C = 1.2	98.6	—	89
Microreactor	Isothermal multichannel microreactor with 16 parallel mini channels	275 °C, 1 bar, S/C = 1.3, and WHSV = 0.67 h^{-1}	89.7	—	90
Microreactor	Non-isothermal microreactor with parallel microchannels and the catalyst coated on the reactor's wall	500 °C, 1 bar, S/C = 10, and GHSV = 24 000 mL (g^{-1} h^{-1})	97.0	—	91
Microreactor	Isothermal microreactor based on 5 stacked wave sheets and copper foam	280 °C, 1 bar, and S/C = 1.5	65.0	—	92
Microreactor	Non-isothermal multilevel series scaled-up microreactor with 5 parallel MeOH combustion chambers	320 °C, 1 bar, and S/C = 1.3	92.5	—	93
Microreactor	Microreactor with a Ti porous membrane of 25 mm diameter and 1 mm thickness	360 °C, 1 bar, S/C = 8.8, and WHSV = 9.28 h^{-1}	63.0	—	94

compared to other transition metals such as Pt, Pd and Co that convert MeOH to CO, on Ni_2P, the MSR reaction may compete with MeOH decomposition. The presented mechanism suggests that formaldehyde (CH_2O^*) reacts with the co-adsorbed OH^* to produce CH_2OOH^*, which is then dehydrogenated to form CO_2. It was also reported that the exceptional selectivity and the coke formation resistance of Ni_2P could potentially be considered as a possible alternative solution for Cu-based catalysts.

4. Main experimental setups and reactors

The reactor configurations play a vital role in the performance of the MSR reaction and more specifically to the conversion of the reaction. The conventional reactor unit that is more frequently utilised for the MeOH-involved H_2 production in thermocatalysis is the packed bed reactor. However, during recent years, efforts were made to develop other reactor designs such as membrane reactors (MR) and micro-reactors to enhance the H_2 production.[66] The smaller reactor units require better design deployment compared to the conventional units to avoid large pressure drops.[67] According to Iulianelli et al.,[68] most of the time, the MSR reactors and MR are tubular in order to compete with the better performance of more complex designs that have higher manufacturing costs. Table 2 summarises different reactor configurations utilised for MSR.

4.1. Packed bed reactors

A packed bed reactor loaded with solid catalytic particles is considered a simple system with low cost of manufacturing and operation. At the industrial level, they are preferred due to their easier design and construction, but at the same time there is a high pressure drop over the reactor.[69] However, proper optimisation of operating conditions of packed bed reactors can significantly improve the H_2 efficiency at the outlet. There have been many studies, recently, focusing of the packed bed reactor units conducting either experimental or theoretical investigations.[70–75]

Karim et al.[76] compared an isothermal packed bed reactor and a coated-wall reactor, where the catalyst bed is a layer in contact with the wall of the reactor. Generally, the benefits of this reactor configuration vary. Some of the advantages are low-pressure drop, better heat and mass transfer and the lowest amount of catalyst to operate.[77] In the packed bed reactor, it was found that between 1 and 4.1 mm internal diameter the heat transfer is limited and temperature gradients of up to 40 K could exist in the reactor bed. In contrast, the coated-wall reactor was free from any heat or mass limitations with lower pressure drop over the reactor and higher catalytic activity. The fact that MeOH can be reformed at low temperatures between 200 and 250 °C makes it even more attractive for large-scale applications.[76]

Hafeez et al.[78] carried out a similar theoretical study comparing the isothermal packed bed and coated wall micro-reactors using a $CuO/ZnO/Al_2O_3$ catalyst (BASF F3-01), which is shown in Fig. 5a and b. Both microreactors appeared to have the
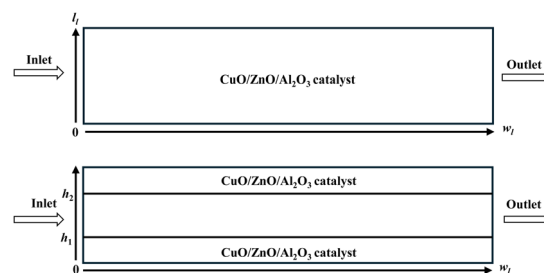

Fig. 5 Schematic representation of the reforming reactor: (a) packed bed and (b) coated-wall packed bed microreactors.[78] Reproduced from ref. 78 with permission from the Royal Society of Chemistry.

similar performance at same temperatures due to the smaller scale of reformers. The coated wall reactor was expected to obtain higher conversion rates at a constant wall temperature in each layer, but the difference between the results of the two reactors was negligible due to the small size of reactors. The test regarding the robustness of the model by a comparison between 2D and 3D modelling configurations confirmed the model validity. Case studies such as the effect of residence time, temperature, steam to MeOH ratio, and thickness of catalyst coating on MeOH conversion were performed. More studies occurred, revealing that the bigger pellet sizes of catalyst led to the appearance of internal mass transfer resistance, followed by a reduction in MeOH conversion.

A numerical investigation was conducted by Kusumastuti et al.[79] using a heating counter-flow tubular packed bed reactor. The tube design is extensively discussed in the literature for its straightforward construction. Three different configurations were assessed for their MSR reaction performance (straight tube, divergent tube and convergent tube), showing that the divergent design achieved the higher MeOH conversion (around 68%). Also, it highlighted the positive effect of internal heating with a waste heat source due to the endothermic reaction which dominates, enhancing the MeOH conversion. The number of heating tubes was another parameter that was investigated varying from 4 to 6 and to 8. The results demonstrated that a higher heating tube number tends to increase the conversion rate as improved heat transfer is accomplished. Additional studies were done to optimise the reactor design such as the position of the heating tube, the reformer angle and the inlet temperature, revealing that the best performance (almost 95% MeOH conversion) was obtained using the divergent shape with 8 heating tubes, a hot air inlet velocity of 0.5 m s^{-1}, a heating tube position of 3.5 mm and a reformer angle of 5° with an inlet temperature of 513 K.

Another limitation that constitutes an obstacle for fuel cell applications and a frequent difficulty to be overcome in packed bed reactors is the irregular temperature distribution. A tubular fixed bed reactor with simultaneous external and internal heating was investigated by Zhang et al.[80] to enhance the temperature distribution and hence the conversion of MeOH. A 3D validated model was utilised to simulate a tubular fixed bed reactor, a tubular fixed bed reactor with an inner heating pipe and a tubular fixed bed reactor with helical fins around the

heating pipe. It reported the significant contribution of the heating pipe in the MeOH conversion and H_2 production. Moreover, the addition of helical fins enhanced the convective heat transfer and flow path of reactants, achieving better performance of the reaction with an increase in the conversion of around 8.5%. It also examined the impact of geometric parameters, such as the pitch, height and width of helical fins, temperature, S/C molar ratio and inlet flow velocity, on the reaction performance. The optimum operating parameters showed almost 100% MeOH conversion.

A 3D numerical model of tubular packed bed reactor comprising several cylindrical tubes was utilised by Wang et al.[81] for the MSR reaction. Effects of various parameters such as S/C molar ratio, inlet temperature, reactant mass flow rate, catalyst particle size and porosity were investigated for assessing the performance of the MSR reaction. The optimised conditions were determined as a temperature of 280 °C, S/C ratio of 2, inlet gas velocity of 0.065 m s^{-1} and catalyst particle size and porosity of 1 mm and 40%, respectively. The catalyst was located in different sections in order to avoid the formation of hot-spot areas inside the reactor in a large extent, especially in a segmented reactor configuration where the temperature inhomogeneity was reduced by almost 70% as well as the CO concentration by over 30%.

Zhu et al.[82] examined the MSR reaction using a $Cu/ZnO/Al_2O_3$ catalyst in a non-isothermal multi-tubular packed-bed reactor with heating tubes operating as a heat exchanger as well. A comprehensive pseudo-homogeneous model was developed, and the validation was conducted following a previous study of Zhu et al.[95] Two different flow set-ups have been investigated. A co-current design in which the reactant and air flow are in the same direction and a counter-current design where both flows are directed in opposite directions. The results demonstrated that both reactors showed high MeOH conversion over 95%, while the co-current design achieved the lowest CO concentration at the outlet of the reactor (0.34%). Additional investigations were carried out for the same catalyst mass by increasing the tube number while decreasing their diameter. An improvement in the MeOH conversion rate was obtained, but at the same time the amount of CO generated was increased.

In order to find applications, the MSR technology should be subject to an economic evaluation for its efficiency and feasibility. Choi and Stenger[96] performed an economic evaluation of an optimized system with the optimized reactor size and operating conditions, using economic profit as the objective function. Here, profit is defined as the difference between H_2 revenue and the fixed and operating costs of production. H_2 revenue is affected by H_2 purity, while reactor and energy costs are also important factors. MATLAB software was utilized for the analysis, where the profit function was maximized by minimizing the difference between cost and revenue through the optimized process.

A technoeconomic analysis by Rahatade and Mali[97] was reported for the first time, considering the integration of heat and steam reforming processes of methanol (MeOH) and dimethyl ether (DME). A fixed-bed reactor was utilized in the simulations at a temperature of 250 °C and a pressure of 20 bar. The economic analysis was conducted by estimating the Total Annual Cost (TAC) of the process, which includes both the fixed capital investment (FCI) and working capital investment (WCI). The results indicated that the utilization of MeOH was cheaper than DME, as fewer utilities were involved. Moreover, heat integration was found to be more beneficial than a non-heat-integrated system, resulting in a reduction in TAC of up to $1610, while H_2 production was approximately $10 300 cheaper than that from DME.

The majority of publications focused on kinetics, thermodynamics, modelling and simulation studies, as well as on evaluating the performance of different reactor designs. However, the technoeconomic analysis of different configurations for the MSR reaction is limited in the literature.

4.2. Membrane reactors

The recent development of PEMFCs as an alternative energy conversion technique aimed to eliminate greenhouse emissions and furthermore environmental pollution that originated from the conventional energy sources.[98] This technology demands high clarity of H_2, which can be achieved by membrane reactors (MRs). A membrane plays a vital role in the removal or addition of chemical species in a reaction system while also contributing to better interactions between the catalyst and reactants without conducting any separation process.[99] These reactors can achieve higher conversions or the same conversion under milder conditions than conventional reactor systems. Moreover, high-purity H_2 production is achieved in a sole unit. The high cost, low chemical resistance in the case of dense Pd-MRs, not high purity H_2 production and perm-selectivity in the case of composite Pd-based MRs and the contamination of H_2S and CO are some of the drawbacks of MRs.[100]

Since Pd-MRs are the most studied ones, Shi et al.[83] developed a Pd membrane reaction system for pure H_2 production. The double-functioned system allowed the low-temperature MSR reaction and the high-temperature purification conducted under isothermal conditions. Experimental results with optimisation revealed that high H_2 purity (above 99.99%) was achieved for a MeOH flow rate between 1 and 2 g min^{-1} and pressure of 1.5–6 bar. Successful separation was achieved with ppm levels of CO concentration and furthermore showed potential to provide up to 500 W, finding application to power mobile devices and small range-extended vehicles.

A high H_2 purification process was designed by Wang et al.[84] for the production of pure H_2 from the MSR reaction using the $CuCe/Al_2O_3$ catalyst and a Pd membrane supported on porous ceramic. Fig. 6a illustrates the schematic diagram of the H_2 integrated MR. Characterisation techniques revealed the exceptional catalyst properties of high catalytic activity and stability. The H_2-purification integrated reactor was operated at temperatures between 360 and 400 °C, showing an increase in the H_2 generation, while MSR was conducted in a wide temperature range between 220 and 400 °C. At 400 °C the H_2 concentration reached a maximum of almost 99.4%, and the CO concentration was found to be around 0.07 vol%. It was reported that the further increase of temperature over 400 °C,
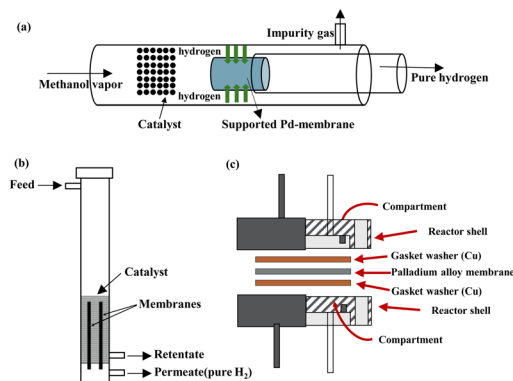
Fig. 6 Schematic representations of MRs with the (a) ceramic supported Pd membrane,[84] (b) Pd–Ag metallic active layer,[87] and (c) Pd–Cu alloy membrane.[101] (a) Reproduced from ref. 84 with permission from Elsevier, Copyright 2023. (b) Reproduced from ref. 87 with permission from Elsevier, Copyright 2022. (c) Reproduced from ref. 101 with permission from Pleiades Publishing Ltd, Copyright 2020.

could lead to intermetallic diffusion between the Pd membrane and stainless-steel support, thereby decreasing the H_2 permeance. In this study, the integrated reactor showed an exceptional stability performance for over 720 min with a high H_2 concentration of above 99%.

Ghasemzadeh et al.[85] investigated and evaluated the application of silica and Pd–Ag MRs in the MSR reaction. The CFD results show that both MRs have rather better performance than the conventional reactor, with the silica MR being the best choice. Also, it is evident that there are lower CO levels at the reactor effluent for the silica membrane as it is more permeable to H_2, which emphasises the shift effect of the reaction, allowing higher MeOH conversion and a higher yield. Under isothermal conditions of 513 K and 5 bar, which was considered the optimum pressure for operation, the H_2 yield was around 95%, while the temperature effect showed an increase in the H_2 yield from 74 to 89% for temperatures between 493 and 573 K. Moreover, an increase in CO selectivity up to 2% was noted for the maximum operated temperature.

Further studies were performed by Ghasemzadeh et al.[86] to assess the performance of different silica isothermal MR configurations. The examined configurations included a co-current flow design, a counter-current flow design and a counter-current flow design including the WGS reaction in the permeate side. All the investigated designs were found to outperform the conventional packed bed reactor. The H_2 purity was one of the goals of this work, and it was analysed in the retentate and permeate streams of all the MR configurations. The counter-current flow design with the WGS reaction in the permeate side showed a better H_2 permeation driving force compared to the other two configurations as well as a lower CO selectivity.

Cifuentes et al.[87] studied the same reaction in a non-isothermal catalytic MR using Pd–Ag metallic membranes and a PdZn/ZnAl$_2$O$_4$/Al$_2$O$_3$ catalyst (Fig. 6b). The MR design was compared with a convectional packed bed reactor, whereas a 3D CFD non-isothermal model was designed and validated using

experimental results including the mass transfer resistances. The experimental results demonstrated an exceptional H_2 recovery of 85% at a temperature of 430 °C and an absolute pressure of 6 bar. Additionally, different operating conditions were evaluated to overcome the heat and mass transfer issues occurring in the reactor.

A study including a Ni–Cu catalyst was performed in a conventional reactor and MR by Mironova et al.[101] It revealed that the H_2 yield in the membrane is higher, and also the Pd–Cu alloy membrane exhibits high H_2 permeability. The schematic representation of the MR is presented in Fig. 6c. Additionally, the membrane provides a high-purity H_2 production (>97%), as a stream of pure H_2 is collected in the permeate zone. An experimental investigation for the permeability of the membrane was conducted, showing that the increase of temperature significantly improved the H_2 recovery rate up to 60%, while the heating from 300 to 400 °C showed great improvement in the H_2 flux across the membrane. During the cooling period, the H_2 flux across the membrane was found to be beyond that observed during the heating period for the same temperatures, attributed to the inhibition of phase transition from α to β upon modification of the Pd–Cu alloy, and thus the phase ratio varied with the increase or decrease of temperature.

Saidi[88] evaluated the performance of a Pd–Ag catalytic membrane for pure H_2 production using a commercial Cu/ZnO/Al$_2$O$_3$ catalyst. A 2D non-isothermal model was designed incorporating all the heat and mass transfer phenomena taking place in the MR, with the simulated results to be in a good agreement with the experimental ones. The effects of pressure, temperature, sweep ratio, and steam ratio on MeOH conversion and H_2 recovery were also examined. The results revealed that the H_2 recovery is enhanced with the temperature and pressure along the reactor length. The selective H_2 removal shifts the reaction equilibrium towards the H_2 formation, hence enhancing the conversion of the reaction. The model showed that at 2 bar, 573 K, and a sweep ratio of 1, the maximum H_2 yield improved from 64% to 100% by increasing the steam ratio from 1 to 4.

The Pd membranes might be considered one of the most expensive membranes, but compared to other materials of lower cost, such as polymer membranes, they offer excellent H_2 recovery and purity over 99% in most of the cases. At the same time, they suffer from embrittlement effects and low thermal and chemical resistances. However, their integration with metals could potentially improve their performance.[102] MRs have a great opportunity for industrial applications as they offer a better solution for high MeOH conversion and high-purity H_2 production compared to packed bed reactors as well as the simultaneous production and separation of reactants and products. Moreover, their lower mechanical and chemical stability and high cost could affect their industrialisation.

MRs are considered appropriate for MSR reaction systems as a plethora of investigations regarding the exceptional reactor's performance and H_2 yield exist in the literature. Nevertheless, the focus of the most publications was to evaluate the performance of new catalytic materials and reactor designs as well as mechanistic and thermodynamic investigations. Therefore, the

techno-economic analysis of the MSR reaction, studying the economic aspects of different scale systems, is limited.[103] Byun et al.[104] conducted a techno-economic analysis to assess the technical and economic feasibility of a packed bed reactor with membrane filters compared to a conventional membrane reactor. Aspen HYSYS software was utilized to investigate the impact of several techno-economic parameters. The analysis employed itemized cost estimation, where a unit's H_2 production cost was calculated by dividing the total cost—defined as the sum of annualized capital cost ($ per year) and operating cost ($ per year)—by the total H_2 production rate (kg per year). It was found that temperature had a significant influence on the reactor performance. The effect of H_2 permeance showed similar results to the temperature effect, where lower unit H_2 production costs could be obtained with higher H_2 permeance. Moreover, it highlighted that a higher number of packed bed reactors and membrane filters do not necessarily assure cheaper H_2 production costs at high temperatures where almost 100% of MeOH is converted.

A similar study was carried out by Kim et al.,[105] who designed a reactor in Aspen HYSYS software to evaluate the technical and economic feasibility of an MR for ultra-pure H_2 production. A unit H_2 production cost was calculated by dividing the annual cost ($ per year) by the annual H_2 production yield (kg H_2 per year), comparing the MR with a conventional packed bed reactor based on process simulation results. The total annual costs for a packed bed reactor and the MR were $93 401 per year and $72 305 per year, respectively, with the capital cost of a membrane module being $5105. Furthermore, the capital expenditure (CAPEX) results demonstrated that CAPEX accounts for 3% in the MR, in contrast to 17% in the packed bed reactor, mainly due to the elimination of the pressure swing adsorption system in the MR. Itemized cost estimations revealed a unit H_2 production cost of $9.37 per kg H_2 for the packed bed reactor and $7.24 per kg H_2 for the MR, respectively, showing approximately a 23% cost reduction in the MR.

4.3. Microreactors

The design of micro-reformers to convert hydrocarbon fuel to H_2 has gained the interest of many scientists. Microchannel reactors provide a powerful tool for process intensification and microscale processing. These reactors are ideal for fast, high exothermic reactions, and they show superior heat and mass transfer rates.[106] The structure and the design of microreactors affect their performance and hence the conversion of MeOH.[107,108] However, despite their advantages, microreactors face challenges that limit their broader application. Their rigid structure reduces flexibility, making it difficult for them to adapt to dynamic environments or fit into limited spaces.[109] Nevertheless, numerous studies in the literature highlight the exceptional performance of microreactors, which often surpasses that of conventional reaction units.[110–114]

Lu et al.[115] investigated three types of microreactors to enhance the direct microchannel performance. Using numerical simulations, the results showed that the sinusoidal microchannel with dimples (SMD) is the optimal structure. In addition, the effects of reaction temperature, MeOH-feeding flux, and steam/MeOH mole ratio on microreactor's performance were examined, while different structures were investigated experimentally for the validation of the results. The SMD microreactor not only showed the best overall performance but also demonstrated significant improvements in heat and mass transfer, along with a high hydrogen production capacity.

A theoretical work focusing on the channel structures of microreactors was conducted by Liu et al.[89] to address issues related to mass and heat transfer phenomena and improve the H_2 yield. Five different channel structures were investigated, involving circle–triangle, circle–square, square–circle, square–square and triangle–circle designs (Table 3). Among these, the circle-triangle design exhibited the best performance, achieving methanol conversion rates above 98% and hydrogen selectivity exceeding 88%. The superior performance of the circle–triangle configuration was attributed to its larger coating area, which improved methanol conversion, and its enhanced its mass transfer rates, resulting from a more efficient velocity flow distribution compared to other channel designs.

Zhuang et al.[90] created a theoretical model to study the MSR reaction in an isothermal multichannel reactor. A commercial $CuO/ZnO/Al_2O_3$ catalyst was utilised in the investigation of sixteen parallel mini-channels. The 3D model accounted for heat and mass transfer within the reactor, providing accurate predictions for species consumption and generation, which were validated through experimental comparisons. The results showed minimal temperature differences (around 2.5 K), demonstrating uniform temperature and fluid velocity distribution across the sixteen parallel mini-channels, indicating the excellent performance of the micro-reactor.
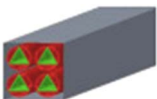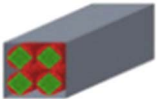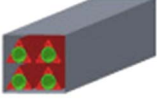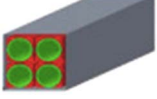
Sarafraz et al.[91] performed the MeOH-involved H_2 production in a non-isothermal microreactor with parallel channels using a $Cu–SiO_2$ catalyst coated on the wall surface. The experiments occurred at operating temperatures of 250–400 °C, reactant flow rates between 0.1 and 0.9 L min^{-1}, catalyst loadings of 0.25–1.25 g and a heat flux value of 500 kW m^{-2}. However, the reactor has an operating tolerance up to 600 °C. An increase of reactants' gas hourly space velocity (GHSV) causes a reduction in conversion, which is due to the lower residence time, the suppression in diffusion of reactants into the pores of the catalyst and also the temperature of the average film. The MeOH conversion can reach 97% at 400 °C at a GHSV of 24 000 mol g^{-1} h^{-1} and a MeOH/water ratio of 1.

Wu et al.[92] suggested an isothermal microreactor with stacked wave sheets and copper foam for highly efficient H_2 generation from MSR. A fractal body-centred cubic model was used to study the flow characteristics and reaction performance of the copper foam with a coated catalyst layer. Experimental and theoretical results revealed that the reformate flow rate increased with the increase of the number of microreactor layers and the flow rate of MeOH. Both studies showed good agreement with only 7% differences in MeOH conversion. It was also observed that the stacked wave sheets and copper foam show a uniform reactant flow and improved H_2 generation.

A scaled-up amplified non-isothermal microreactor was designed by Wu et al.[93] to enhance the production of H_2.

Table 3 Five different channel structures.[89] Reproduced from ref. 89 with permission from Elsevier, Copyright 2024

Channel type	Overall shape	Cross-sectional shape	Catalytic coatings	Combustion channel
Circle–triangle				
Circle–square				
Triangle–circle				
Square–circle				
Square–square				

Experimental and theoretical studies were conducted, where 5 MSR plates were used along with 5 MeOH combustion chambers to improve the distribution of temperature. The velocity distribution within the microchannels and Cu foam showed better homogeneity in the first case. The microchannels and Cu foam combination resulted in better mixing of reactants. In addition, as the reforming chambers are uniformly designed, the flow velocity is symmetrically distributed. The results from MeOH combustion and MSR reaction showed that the microreactor was heated from 18.5 to 310 °C within 1618 seconds. Optimal operating conditions resulted in methanol conversion rates above 88%.

Fan *et al.*[94] developed a membrane microreactor for the MeOH-involved H_2 production using immobilised Cu/ZnO/Al_2O_3 nanoparticles in the pores of the membrane. Characterisation techniques verified that the nanoparticles were successfully immobilised. A comparison with a conventional packed bed reactor was conducted with the membrane microreactor to show an exceptional performance (5000 mmol h^{-1} H_2 yield) which was one order of magnitude higher than that of the packed bed reactor. Additional investigations showed that there is no concentration gradient, and hence the velocity is uniformly distributed resulting in almost 100% H_2 selectivity. It predicted that by stacking five membrane microreactor sheets, methanol conversion could exceed 95%.

A numerical modelling study of the MSR reaction in a heterogeneously catalysed microchannel SR reactor was conducted by Chen and Yu.[116] The main goal of the study was to investigate the phenomena occurring within the microchannel reactor during the reactions. The effects of various parameters were evaluated to enhance the reactor's performance. The results indicated that mass transfer resistance was present despite the system's small scale, suggesting that design improvements are necessary to eliminate external mass transfer limitations. A maximum output power in excess of 70 W per channel was achieved, and energy efficiencies of up to approximately 70% were available. The operating limit line of MeOH breakthrough was found to influence the H_2 yield, while an optimum velocity, along with adjustments to the flow rate and catalyst loading, was necessary to control and achieve high MeOH conversions.

Zhuang *et al.*[117] experimentally investigated the performance of a novel isothermal multichannel micropacked bed reactor with a bifurcation inlet manifold and a rectangular outlet manifold. A commercial CuO/ZnO/Al_2O_3 catalyst was utilized to assess the effects of different parameters on MeOH conversion, H_2 production, and CO concentration. The results demonstrated that temperature had a more significant impact on the reaction's performance compared to the S/C ratio and weight hourly space velocity (WHSV). Moreover, an improved MeOH conversion rate was obtained by increasing the S/C ratio and temperature while decreasing the WHSV and particle size. The reactor was suggested to be suitable for Proton Exchange Membrane Fuel Cell (PEMFC) applications for H_2 production under operating conditions of an S/C ratio of 1.3, a temperature of 275 °C, a WHSV of 0.67 h^{-1}, and a particle size between 150 and 200 mesh, achieving over 94% MeOH conversion and a CO yield of less than 1%.

Membrane reactors and microreactors present a promising alternative to conventional packed bed reactors for MSR, offering high hydrogen purity and conversion rates under milder conditions, as well as improved heat and mass transfer.

However, cost remains a significant barrier for membrane reactors, despite their ability to integrate a reformer and a separator into a single unit, which could potentially lead to lower operating temperatures compared to conventional reactors. As noted by Kim *et al.*,[105] comprehensive studies that combine both process simulation and economic analysis are scarce in the literature. Therefore, greater emphasis should be placed on the economic analysis of MRs to assess their economic feasibility. Furthermore, the MSR reaction operates at relatively low temperatures between 200 and 300 °C, as shown in Table 2, making it a competitive and attractive candidate for various applications. Additionally, strategies aimed at lowering the activation barrier of the reaction could further reduce operating temperatures, enhancing the viability of MSR systems. More research on scaling up microreactors is required to ensure that their advantages, such as uniform distribution, are maintained in industrial applications. Optimizing reactor designs for methanol reforming, especially for industrial uses, is crucial as current investigations are limited.

5. Integration of the MSR reaction and fuel cell systems

Recent trends in the literature show that the fuel cell technology is a promising alternative for the elimination of emissions of commercial vehicles. Challenges that must be overcome are often ascribed to the high manufacturing cost. In order to compete the existing technologies and increase the demand, different strategic decisions must be considered by the manufacturing companies and the states.[118] Fuel cell techniques can be separated into 5 types, the PEMFCs, alkaline fuel cells (AFCs), phosphoric acid fuel cells (PAFCs), molten carbonate fuel cells (MCFCs) and solid oxide fuel cells (SOFCs). Among the different kind of techniques, the most popular one is the PEMFCs.[119] Ideally, membranes used in PEMFC systems should target the high conductivity of protons, low electronic conductivity, low fuel permeability, low drag coefficient of

electroosmotic, good thermal/chemical stability and mechanical properties.[120] The PEMFC system structure consists of bipolar plates, gas diffusion layers on both sides and a PEM in the middle of the configuration. Fig. 7 illustrates the proton formation and transportation from the anode to the cathode through the PEM to react with O_2, producing electrons and hence water, electricity and heat.[121]

There are two categories of PEMFCs divided based on the temperature level of operation, low-temperature PEMFCs (LT-PEMFCs) and high-temperature PEMFCs (HT-PEMFCs), operating around 60–80 °C and 160–220 °C, respectively. Because of the low CO tolerance of LT-PEMFCs, this system faces poisoning issues at the catalyst anode simultaneously and thus the HT-PEMFCs are more advantageous,[122] offering emission free conversions and simplified water and heat management and cooling systems. However, HT-PEMFCs due to their high operating temperatures carry safety risks and technical challenges and also incur high manufacturing costs.[123] On the other hand, the reforming LT-PEMFC systems have high power density and proton conductivity as well as low heat loss, making it suitable for portable small-scaled devices.[124] According to Ribeirinha *et al.*,[125] the membrane composition plays a vital role in CO tolerance since polybenzimidazole (PBI) membranes and generally most of the PEMs can tolerate CO concentrations up to 3000 ppm and can be straightaway fed with MeOH stream without any purification process. It was also noted that the heat recovery is important during the operation to maximise the overall efficiency.[126]

An experimental and a theoretical investigation were performed by Ribeirinha *et al.*,[127] using an integrated HT-PEMFC with a cellular membrane packed bed reactor. Fig. 8a illustrates the integrated system showing all the constituent parts. The Pd–Ag membrane on the reaction unit was employed, showing H_2 permeability to suspend the poisoning of the anode by MeOH. However, the Pd–Ag membrane deactivation due to CO adsorption is less noticeable at lower temperatures. A 3D non-isothermal model was designed successfully, and Ansys Fluent software was used to validate the experimental results. The integrated designed configuration showed similar performance to that of the HT-PEMFC system fed with pure H_2. Moreover, heat integration and heat efficiency were used from the electrochemical reaction to the MSR reaction.

Liu *et al.*[128] developed a model designing a tubular HT-PEMFC integrated with a built-in packed bed reactor for the MSR reaction. The model was designed using COMSOL Multiphysics, including all the mass, heat and momentum equations as well as the MSR reaction, WGS reaction and MeOH cracking reaction, and was validated with experimental results showing good agreement. The main goal of the work was to assess the performance of the reaction and the thermal behaviour with various operating parameters. The results demonstrated that the reduction of voltage resulted in electrochemical heat production affecting the temperature distribution. Moreover, on the MeOH conversion, the voltage effect was studied for external potentials between 0.4 and 0.9 V, revealing that above 0.75 V there is no difference in the MeOH conversion values attributed to the low electrochemical heat production. For
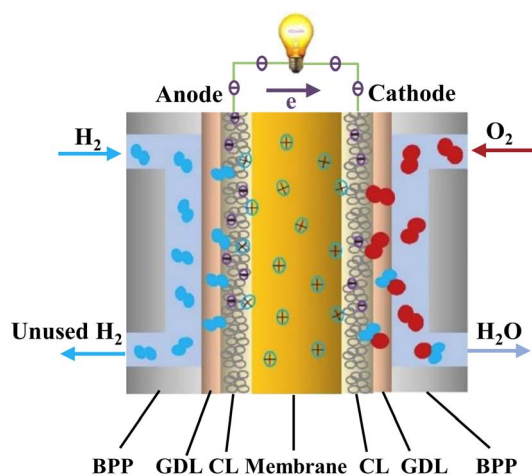

Fig. 7 PEMFC schematic illustration.[121] Reproduced from ref. 121 with permission from Elsevier, Copyright 2023.
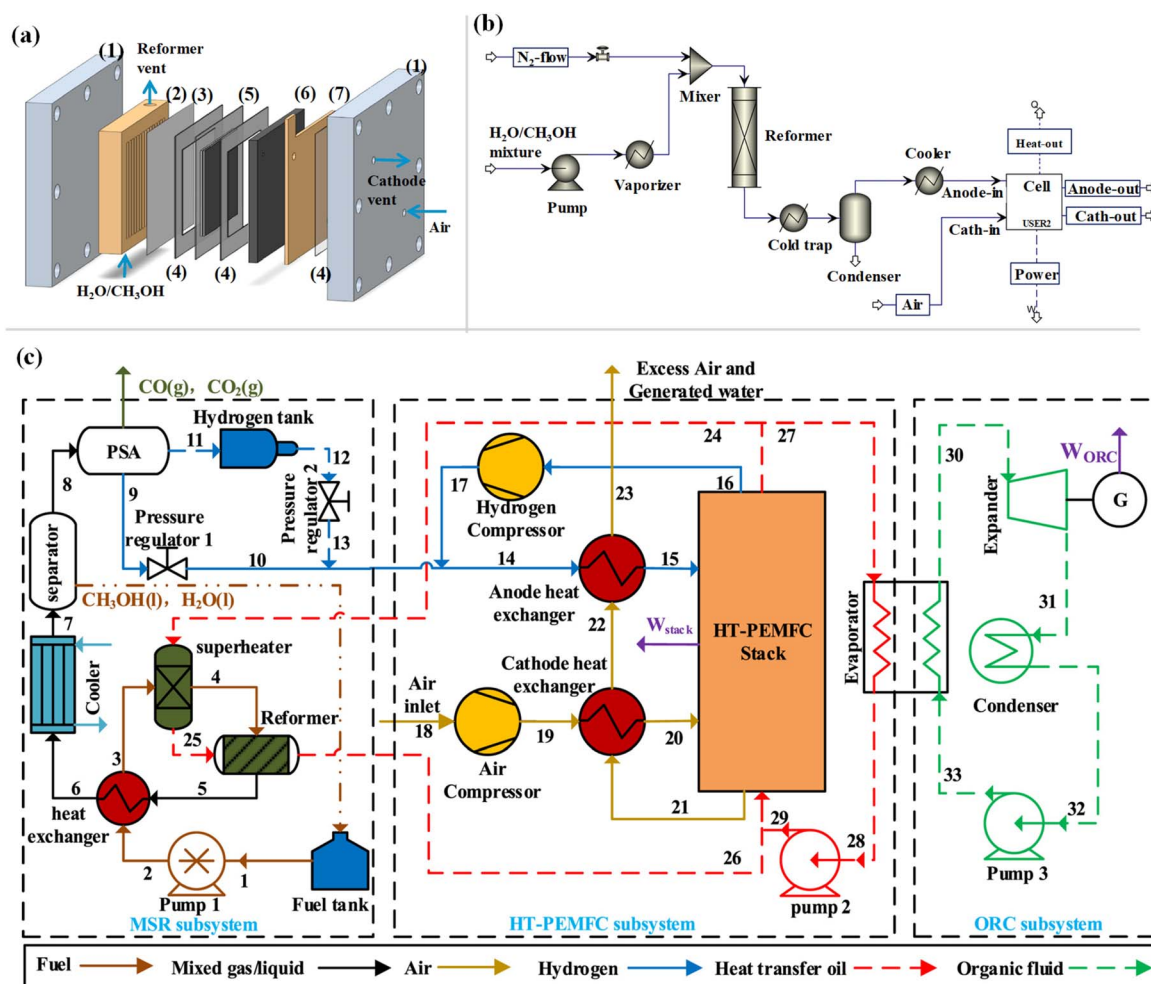
Fig. 8 (a) Representation scheme of the cellular membrane packed bed reactor integrated with a HT-PEMFC: (1) metal end-frame plates, (2) gold coated reformer, (3) Pd–Ag membrane, (4) gasket, (5) MEA, (6) bipolar graphite plate and (7) current collector.[127] (b) Flowsheet diagram of the integrated fuel cell system[130] and (c) schematic diagram of the HT-PEMFC system integrated with an MSR reactor setup and an ORC subsystem.[131] (a) Reproduced from ref. 127 with permission from Elsevier, Copyright 2018, (b) reproduced from ref. 130 with permission from Elsevier, Copyright 2023, and (c) reproduced from ref. 131 with permission from Elsevier, Copyright 2022.

voltage values of 0.5 and 0.55 V, the MeOH reforming rate was found to be enhanced compared to that of the isothermal conditions achieving around 98% and 94%, respectively. Thus, the electrochemical heat can satisfy the required heat for the MSR reaction.

Chen *et al.*[129] designed a 0D model including both MSR and HT-PEMFC technologies and studied the influence of different parameters such as the S/C ratio, reaction temperature, fuel cell number, MeOH catalytic combustion ratio and anode stoichiometry on the system efficiency and performance. As stated by this and many other studies, great effort must be put into enhancing the power generation. The optimisation of the S/C ratio should be made considering the CO selectivity, revealing that the S/C ratio of 1 had the highest CO selectivity. Maximum output power was obtained at 513 K with the efficiency increasing up to 37% compared to other reaction temperatures. Additionally, the anode reduction stoichiometry led to efficient electricity generation of almost 12%. The integrated system was able to sustain the heat generation from the anode.

A kinetic analysis of the MSR reaction on a commercial Cu/ZnO/Al$_2$O$_3$ catalyst and a theoretical study concerning the integration of the MSR reaction and HT-PEMFC were conducted by Ozcan and Akin,[130] as shown in Fig. 8b. The system was developed for portable devices with power less than 15 W under optimum conditions. Using all the reaction rates and kinetics obtained from the analysis, a comparison was carried out between the obtained experimental and simulated conversion rates, showing good agreement between the results. The results from investigating different operating conditions in order to optimise the net power output of the integrated system were evaluated revealing that the system could generate 15.4 W power output, which is about twice that of the total required power (6.2 W).

A novel approach for an integrated system was suggested by Li *et al.*,[131] suggesting the utilisation of heat waste from the HT-PEMFC system to supply the MSR reaction for H$_2$ generation. An organic ranking cycle (ORC) was proposed as well, to recover the remaining heat for electrical power generation (Fig. 8c). A

thermodynamic model was designed, and the results showed that the reaction rate was enhanced by the increase of temperature and the H_2O/MeOH ratio, achieving a H_2 yield above 95%. In addition, the implementation of the ORC subsystem using R245fa as the organic working fluid for waste heat recovery showed that the system has a better performance with the highest net output power of 1.64 W and efficiency of 17.65%. It was observed that higher anode pressures and hence lower cathode pressures could potentially improve the thermodynamic performance, minimising the cost and environmental pollution. The system optimisation resulted in an increase of net power output by around 48%.

Liang et al.[132] incorporated a waste heat system that could be used in combination with cooling, heating and power generation for the integrated MSR-PEMFC system. An equation-oriented framework for the optimisation of the combined cooling, heating and power generation was proposed. The framework included the modelling of the MSR reaction and PEMFC system in detail, cooling and heating systems, heat integration, heat exchangers and energy and economic performance evaluation. It showed that the combined heating, cooling and power system was economically and thermodynamically advantageous to heat recovery. Moreover, the combination system showed 4.5% levelised cost of electricity of 0.2374 $ per kW per h compared with the conventional combination system. The heat exchanger network consists only about 2% of the total investment being effective in reducing the computational complexity.

6.   Challenges & prospects

There is growing interest in the MSR reaction and more generally to MeOH for its importance as a chemical, fuel and feedstock. MeOH is one of the key H_2-carrier molecules, with potential applications in the transportation sector. However, the technology faces several challenges, particularly in catalyst development. Effective catalysts must inhibit CO formation while increasing selectivity towards H_2 and CO_2. This is crucial not only to prevent catalyst deactivation but also to avoid poisoning the anode in PEMFCs. The design of such catalysts should focus on optimizing the performance at lower temperatures to suppress the RWGS reaction, thereby minimizing CO generation. If CO production cannot be completely suppressed, catalysts must be designed with materials that offer resistance to coking, tolerance to poisoning, and stability against sintering, thus extending their operational lifespan. Another key challenge is the high cost of catalyst materials. For example, although Pd-based catalysts have demonstrated exceptional conversion rates and H_2 yields, their high cost hinders widespread adoption in large-scale applications.

A deeper understanding of the MSR reaction mechanism, metal–support interactions, surface adsorption energy, reaction pathways, and energy barriers is essential for developing effective catalysts. Many Cu-based catalysts have been thoroughly studied in terms of their reaction mechanisms, and there has been recent progress with Ni-based catalysts as well. Research on new materials for the MSR reaction should be conducted

strategically, aiming to overcome CO formation and catalyst deactivation through mechanistic studies and the design of cost-effective catalysts for practical applications. Another critical aspect of catalyst design is the pore structure, which can often be random and result in the deactivation of catalytic sites. Proper design of the porous structure, accounting for heat and mass transfer phenomena, can maximize active reaction sites and improve the overall catalyst efficiency.

The selection of operational units is crucial for the traditional packed bed reactor to suffer from hot spots due to the thermal non-uniformity and the large pressure drop over the reactor's length. The reactor and herein the system concept should be able to carry out the MSR reaction in small- and large-scale applications and with high efficiencies. The MRs and micro-reactors are more advantageous compared to the conventional unit. MRs offer the selective separation of component species and could be employed directly to PEMFC units without any purification process, while the micro-reactors can overcome the pressure drop issues of packed bed reactors offering better heat and mass transfer rates. Nevertheless, the Pd membranes that have shown superior separation performance are limited by their enormous cost. Many efforts should be made in order to create cost-effective MRs and microreactors in terms of membrane materials and improve their scalability and operation in order to overcome potential issues.

PEMFC applications in the transportation sector were found to be a promising solution against the conventional fuel combustion engines. The direct utilisation of MeOH in PEMFC systems lacks performance due to the oxidation and poisoning of the anode. However, the transformation of the H_2-energy carrier, MeOH, through the reforming reaction into H_2 is more attractive due to the lower energy density. The main challenge is the heat recovery to maximise the overall efficiency and not waste the released heat from the HT-PEMFC systems. Many investigations suggest the heat integration between the reformer unit and HT-PEMFC to operate at similar temperatures. Another important parameter is the lifetime of the integrated system which most of the times depends on the stability of HT-PEMFC stacks. The optimisation of existing components used and the development of new ones are considered major contributors. Moreover, the lifetime of HT-PEMFC stacks in real-world applications is even more affected compared to the lab-scale experiments as there are many variations in the operating conditions, issues regarding the heat management, cell imbalances and failures. PEMFC systems also face other serious problems such as chemical, mechanical and thermal degradation and agglomeration. The main reason for this effect is the high operating temperatures, the acidic environment and the low humidity, which should be addressed soon in order to facilitate this technology transfer.

Data availability

No primary research results, software or code has been included and no new data were generated or analysed as part of this review.

Author contributions

Conflicts of interest

There are no conflicts to declare.

Acknowledgements

References

1 N. L. Panwar, S. C. Kaushik and S. Kothari, Role of renewable energy sources in environmental protection: a review, *Renewable Sustainable Energy Rev.*, 2011, **15**(3), 1513–1524, DOI: **10.1016/j.rser.2010.11.037**.

2 I. Staffell, *et al.*, The role of hydrogen and fuel cells in the global energy system, *Energy Environ. Sci.*, 2019, **12**(2), 463–491.

3 N. Sazali, Emerging technologies by hydrogen: a review, *Int. J. Hydrogen Energy*, 2020, **45**(38), 18753–18771, DOI: **10.1016/j.ijhydene.2020.05.021**.

4 H. Wang, E. Harkou, A. Constantinou, S. M. Al-Salemc, G. Manos and J. Tang, From photocatalysis to photon-phonon co-driven catalysis for methanol reforming to hydrogen and valuable by-products, *Chem. Soc. Rev.*, 2025, DOI: **10.1039/d4cs00551a**.

5 M. R. Usman, Hydrogen storage methods: review and current status, *Renewable Sustainable Energy Rev.*, 2022, **167**, 112743, DOI: **10.1016/j.rser.2022.112743**.

6 H. Wang, *et al.*, High quantum efficiency of hydrogen production from methanol aqueous solution with PtCu–TiO$_2$ photocatalysts, *Nat. Mater.*, 2023, **22**, 619–626, DOI: **10.1038/s41563-023-01519-y**.

7 G. Garcia, E. Arriola, W.-H. Chen and M. D. De Luna, A comprehensive review of hydrogen production from methanol thermochemical conversion for sustainability, *Energy*, 2021, **217**, 119384, DOI: **10.1016/j.energy.2020.119384**.

8 X. Xu, K. Shuai and B. Xu, Review on Copper and Palladium Based Catalysts for Methanol Steam Reforming to Produce Hydrogen, *Catalysts*, 2017, **7**(6), 183, DOI: **10.3390/catal7060183**.

9 S. Hafeez, *et al.*, Review on recent progress and reactor set-ups for hydrogen production from formic acid decomposition, *Mater. Today Chem.*, 2022, **26**, 101120, DOI: **10.1016/j.mtchem.2022.101120**.

10 M. Niermann, A. Beckendorff, M. Kaltschmitt and K. Bonhoff, Liquid Organic Hydrogen Carrier (LOHC) – Assessment Based on Chemical and Economic Properties, *Int. J. Hydrogen Energy*, 2019, **44**(13), 6631–6654, DOI: **10.1016/j.ijhydene.2019.01.199**.

11 F. B. Juangsa, A. R. Irhamna and M. Aziz, Production of ammonia as potential hydrogen carrier: review on thermochemical and electrochemical processes, *Int. J. Hydrogen Energy*, 2021, **46**(27), 14455–14477, DOI: **10.1016/j.ijhydene.2021.01.214**.

12 P. Adamou, *et al.*, Recent progress for hydrogen production from ammonia and hydrous hydrazine decomposition: a review on heterogeneous catalysts, *Catal. Today*, 2023, **423**, 114022, DOI: **10.1016/j.cattod.2023.01.029**.

13 S. Sá, H. Silva, L. Brandão, J. M. Sousa and A. Mendes, Catalysts for methanol steam reforming—a review, *Appl. Catal., B*, 2010, **99**(1), 43–57, DOI: **10.1016/j.apcatb.2010.06.015**.

14 A. M. Ranjekar and G. D. Yadav, Steam reforming of methanol for hydrogen production: a critical analysis of catalysis, processes, and scope, *Ind. Eng. Chem. Res.*, 2021, **60**(1), 89–113.

15 M. Rostami, A. H. Farajollahi, R. Amirkhani and M. E. Farshchi, A review study on methanol steam reforming catalysts: evaluation of the catalytic performance, characterizations, and operational parameters, *AIP Adv.*, 2023, **13**(3), 030701, DOI: **10.1063/5.0137706**.

16 W.-W. Yang, X. Ma, X.-Y. Tang, P.-Y. Dou, Y.-J. Yang and Y.-L. He, Review on developments of catalytic system for methanol steam reforming from the perspective of energy-mass conversion, *Fuel*, 2023, **345**, 128234, DOI: **10.1016/j.fuel.2023.128234**.

17 A. Iulianelli, P. Ribeirinha, A. Mendes and A. Basile, Methanol steam reforming for hydrogen generation via conventional and membrane reactors: a review, *Renewable Sustainable Energy Rev.*, 2014, **29**, 355–368, DOI: **10.1016/j.rser.2013.08.032**.

18 M. S. Herdem, M. Y. Sinaki, S. Farhad and F. Hamdullahpur, An overview of the methanol reforming process: comparison of fuels, catalysts, reformers, and systems, *Int. J. Energy Res.*, 2019, **43**(10), 5076–5105, DOI: **10.1002/er.4440**.

19 S. S. Mabaleha and P. Kalita, Enhancing Hydrogen Production in Methanol Steam Reforming Using PdZn-Based Catalysts: A Mini-review on CO Suppression, *Energy Fuels*, 2024, **38**(15), 13565–13584.

20 R. Ye, *et al.*, Advances in Enhancing the Stability of Cu-Based Catalysts for Methanol Reforming, *Catalysts*, 2022, **12**(7), 747, DOI: **10.3390/catal12070747**.

21 H. Yu, Y. Li, C. Xu, F. Jin, F. Ye and X. Li, Distinct facets to enhance the process of hydrogen production via methanol steam reforming—a review, *Energy Storage Sav.*, 2022, **1**(1), 53–69, DOI: **10.1016/j.enss.2021.12.001**.

22 W.-H. Chen, *et al.*, Sustainable cement and clay support in Ni–Cu/Al$_2$O$_3$ catalysts for enhancing hydrogen production

from methanol steam reforming, *Int. J. Hydrogen Energy*, 2024, **54**, 267–283, DOI: **10.1016/j.ijhydene.2022.12.015**.

23 A. A. Lytkina, N. A. Zhilyaeva, M. M. Ermilova, N. V. Orekhova and A. B. Yaroslavtsev, Influence of the support structure and composition of Ni-Cu-based catalysts on hydrogen production by methanol steam reforming, *Int. J. Hydrogen Energy*, 2015, **40**(31), 9677–9684, DOI: **10.1016/j.ijhydene.2015.05.094**.

24 P. Tahay, Y. Khani, M. Jabari, F. Bahadoran and N. Safari, Highly porous monolith/TiO$_2$ supported Cu, Cu-Ni, Ru, and Pt catalysts in methanol steam reforming process for H$_2$ generation, *Appl. Catal., A*, 2018, **554**, 44–53, DOI: **10.1016/j.apcata.2018.01.022**.

25 C. Mateos-Pedrero, C. Azenha, P. T. Pacheco, J. M. Sousa and A. Mendes, The influence of the support composition on the physicochemical and catalytic properties of Cu catalysts supported on zirconia-alumina for methanol steam reforming, *Appl. Catal., B*, 2020, **277**, 119243, DOI: **10.1016/j.apcatb.2020.119243**.

26 L. Li, *et al.*, Preparation of CuZnZrAl catalysts by coprecipitation-ammonia method for methanol steam reforming and the effect of promoters Y and Ce, *Mol. Catal.*, 2023, **537**, 112887, DOI: **10.1016/j.mcat.2022.112887**.

27 X. Xu, T. Lan, G. Zhao, Q. Nie, F. Jiang and Y. Lu, Interface-hydroxyl enabling methanol steam reforming toward CO-free hydrogen production over inverse ZrO$_2$/Cu catalyst, *Appl. Catal., B*, 2023, **334**, 122839, DOI: **10.1016/j.apcatb.2023.122839**.

28 Z. Cheng, *et al.*, High-performance Cu/ZnO/Al$_2$O$_3$ catalysts for methanol steam reforming with enhanced Cu-ZnO synergy effect via magnesium assisted strategy, *J. Energy Chem.*, 2021, **63**, 550–557, DOI: **10.1016/j.jechem.2021.08.025**.

29 S. Bepari, M. Khan, X. Li, N. Mohammad and D. Kuila, Effect of Ce and Zn on Cu - Based Mesoporous Carbon Catalyst for Methanol Steam Reforming, *Top. Catal.*, 2023, **66**(5), 375–392, DOI: **10.1007/s11244-022-01772-6**.

30 X. Liu, *et al.*, Cu/REO (RE = La, Pr, Sm, Y, Ce) catalysts for methanol steam reforming: understanding the interaction between Cu and individual REO supports, *Fuel*, 2024, **357**, 130080, DOI: **10.1016/j.fuel.2023.130080**.

31 L. Lin, *et al.*, Low-temperature hydrogen production from water and methanol using Pt/α-MoC catalysts, *Nature*, 2017, **544**(7648), 80–83, DOI: **10.1038/nature21672**.

32 V. Shanmugam, S. Neuberg, R. Zapf, H. Pennemann and G. Kolb, Hydrogen production over highly active Pt based catalyst coatings by steam reforming of methanol: effect of support and co-support, *Int. J. Hydrogen Energy*, 2020, **45**(3), 1658–1670, DOI: **10.1016/j.ijhydene.2019.11.015**.

33 H. K. Huang, *et al.*, Synthesis and regeneration of mesoporous Ni–Cu/Al$_2$O$_4$ catalyst in sub-kilogram-scale for methanol steam reforming reaction, *Int. J. Hydrogen Energy*, 2022, **47**(88), 37542–37551, DOI: **10.1016/j.ijhydene.2021.12.080**.

34 N. Ghaffari Saeidabad, *et al.*, A Review on Catalysts Development for Steam Reforming of Biodiesel Derived Glycerol; Promoters and Supports, *Catalysts*, 2020, **10**(8), 910, DOI: **10.3390/catal10080910**.

35 N. Murakami, T. Chiyoya, T. Tsubota and T. Ohno, Switching redox site of photocatalytic reaction on titanium(IV) oxide particles modified with transition-metal ion controlled by irradiation wavelength, *Appl. Catal., A*, 2008, **348**(1), 148–152, DOI: **10.1016/j.apcata.2008.06.040**.

36 S. Neubert, *et al.*, Highly efficient rutile TiO$_2$ photocatalysts with single Cu(II) and Fe(III) surface catalytic sites, *J. Mater. Chem. A*, 2016, **4**(8), 3127–3138, DOI: **10.1039/c5ta07036h**.

37 A. M. Abiso, O. O. Fasanya, M. Y. Suleiman, A. Y. Atta, J. Dutta and B. E.-Y. Jibril, Advances in copper-based catalysts for sustainable hydrogen production via methanol steam reforming, *Chem. Eng. J. Adv.*, 2024, **19**, 100625, DOI: **10.1016/j.ceja.2024.100625**.

38 L. Chen, *et al.*, Insights into the mechanism of methanol steam reforming tandem reaction over CeO$_2$ supported single-site catalysts, *J. Am. Chem. Soc.*, 2021, **143**(31), 12074–12081.

39 G.-S. Wu, D.-S. Mao, G.-Z. Lu, Y. Cao and K.-N. Fan, The Role of the Promoters in Cu Based Catalysts for Methanol Steam Reforming, *Catal. Lett.*, 2009, **130**(1), 177–184, DOI: **10.1007/s10562-009-9847-8**.

40 N. Iwasa, S. Kudo, H. Takahashi, S. Masuda and N. Takezawa, Highly selective supported Pd catalysts for steam reforming of methanol, *Catal. Lett.*, 1993, **19**(2–3), 211–216, DOI: **10.1007/BF00771756**.

41 K. Ploner, *et al.*, The sol–gel autocombustion as a route towards highly CO$_2$-selective, active and long-term stable Cu/ZrO$_2$ methanol steam reforming catalysts, *Mater. Chem. Front.*, 2021, **5**(13), 5093–5105, DOI: **10.1039/D1QM00641J**.

42 D. Li, *et al.*, Induced activation of the commercial Cu/ZnO/Al$_2$O$_3$ catalyst for the steam reforming of methanol, *Nat. Catal.*, 2022, **5**(2), 99–108, DOI: **10.1038/s41929-021-00729-4**.

43 N. Iwasa, S. Masuda, N. Ogawa and N. Takezawa, Steam reforming of methanol over Pd/ZnO: effect of the formation of PdZn alloys upon the reaction, *Appl. Catal., A*, 1995, **125**(1), 145–157, DOI: **10.1016/0926-860X(95)00004-6**.

44 G. J. Kim, M. S. Kim, J. Y. Byun and S. C. Hong, Effects of Ru addition to Pd/Al$_2$O$_3$ catalysts on methanol steam reforming reaction: a mechanistic study, *Appl. Catal., A*, 2019, **572**, 115–123, DOI: **10.1016/j.apcata.2018.12.035**.

45 B. W. L. Jang, R. Gläser, M. Dong and C. J. Liu, Fuels of the future, *Energy Environ. Sci.*, 2010, **3**(3), 253, DOI: **10.1039/c003390c**.

46 X. K. Gu, *et al.*, Supported single Pt$_1$/Au$_1$ atoms for methanol steam reforming, *ACS Catal.*, 2014, **4**(11), 3886–3890, DOI: **10.1021/cs500740u**.

47 L. Lin, *et al.*, Atomically Dispersed Ni/α-MoC Catalyst for Hydrogen Production from Methanol/Water, *J. Am. Chem. Soc.*, 2021, **143**(1), 309–317, DOI: **10.1021/jacs.0c10776**.

48 S. Bepari and D. Kuila, Steam reforming of methanol, ethanol and glycerol over nickel-based catalysts-a review,

Int. J. Hydrogen Energy, 2020, **45**(36), 18090–18113, DOI: 10.1016/j.ijhydene.2019.08.003.

49 G. Modragón-Galicia, *et al.*, Catalytic Aspects of Pt/Pd Supported on ZnO Rods for Hydrogen Production in Methanol Steam Reforming, *Top. Catal.*, 2022, **65**(13), 1556–1569, DOI: 10.1007/s11244-022-01633-2.

50 L. N. Chen, *et al.*, Efficient Hydrogen Production from Methanol Using a Single-Site Pt_1/CeO_2 Catalyst, *J. Am. Chem. Soc.*, 2019, **141**(45), 17995–17999, DOI: 10.1021/jacs.9b09431.

51 S. Zhang, Y. Liu, M. Zhang, Y. Ma, J. Hu and Y. Qu, Sustainable production of hydrogen with high purity from methanol and water at low temperatures, *Nat. Commun.*, 2022, **13**(1), 5527, DOI: 10.1038/s41467-022-33186-z.

52 J. Zhang, *et al.*, Morphology effect of $Pd/In_2O_3/CeO_2$ catalysts on methanol steam reforming for hydrogen production, *Int. J. Hydrogen Energy*, 2024, **51**, 1185–1199, DOI: 10.1016/j.ijhydene.2023.07.186.

53 Z. Shi, *et al.*, Catalyst, reactor, reaction mechanism and CO remove technology in methanol steam reforming for hydrogen production: a review, *Fuel Process. Technol.*, 2023, **252**, 108000, DOI: 10.1016/j.fuproc.2023.108000.

54 Y. Zhang, *et al.*, Single-atom Cu anchored catalysts for photocatalytic renewable H_2 production with a quantum efficiency of 56%, *Nat. Commun.*, 2022, **13**(1), 58, DOI: 10.1038/s41467-021-27698-3.

55 S. Lin, D. Xie and H. Guo, Methyl formate pathway in methanol steam reforming on copper: density functional calculations, *ACS Catal.*, 2011, **1**(10), 1263–1271.

56 L. Oar-Arteta, *et al.*, Comparison of Noble Metal- and Copper-Based Catalysts for the Step of Methanol Steam Reforming in the Dimethyl Ether Steam Reforming Process, *Ind. Eng. Chem. Res.*, 2016, **55**(12), 3546–3555, DOI: 10.1021/acs.iecr.6b00126.

57 F. Bossola, N. Scotti, F. Somodi, M. Coduri, C. Evangelisti and V. Dal Santo, Electron-poor copper nanoparticles over amorphous zirconia-silica as all-in-one catalytic sites for the methanol steam reforming, *Appl. Catal., B*, 2019, **258**, 118016, DOI: 10.1016/j.apcatb.2019.118016.

58 J. Reyna-Alvarado, O. A. López-Galán, M. Ramos, J. Rodríguez and R. Pérez-Hernández, A theoretical catalytic mechanism for methanol reforming in CeO_2 vs Ni/CeO_2 by energy transition states profiles, *Catal. Today*, 2022, **392–393**, 146–153, DOI: 10.1016/j.cattod.2021.05.009.

59 Z. J. Zuo, L. Wang, P. De Han and W. Huang, Insights into the reaction mechanisms of methanol decomposition, methanol oxidation and steam reforming of methanol on Cu(111): a density functional theory study, *Int. J. Hydrogen Energy*, 2014, **39**(4), 1664–1679, DOI: 10.1016/j.ijhydene.2013.11.048.

60 J. L. C. Fajín and M. N. D. S. Cordeiro, Insights into the Mechanism of Methanol Steam Reforming for Hydrogen Production over Ni–Cu-Based Catalysts, *ACS Catal.*, 2022, **12**(1), 512–526, DOI: 10.1021/acscatal.1c03997.

61 X. Tang, *et al.*, Single Ni-inserted Cu (111) surface: a DFT study of adsorption and reaction mechanisms of methanol steam reforming, *Appl. Surf. Sci.*, 2022, **596**, 153635, DOI: 10.1016/j.apsusc.2022.153635.

62 X. Yang, Mechanistic insights into ruthenium-catalyzed production of H_2 and CO_2 from methanol and water: a DFT study, *ACS Catal.*, 2014, **4**(4), 1129–1133, DOI: 10.1021/cs500061u.

63 X. Wang, D. Li, Z. Gao, Y. Guo, H. Zhang and D. Ma, The Nature of Interfacial Catalysis over $Pt/NiAl_2O_4$ for Hydrogen Production from Methanol Reforming Reaction, *J. Am. Chem. Soc.*, 2023, **145**(2), 905–918, DOI: 10.1021/jacs.2c09437.

64 Z.-W. Xue, *et al.*, Mechanism study on gliding arc (GA) plasma reforming: reaction and energy pathways for H_2 production from methanol steam reforming, *Chem. Eng. J.*, 2023, **462**, 142319, DOI: 10.1016/j.cej.2023.142319.

65 A. Almithn and Z. Alhulaybi, A Mechanistic Study of Methanol Steam Reforming on Ni_2P Catalyst, *Catalysts*, 2022, **12**(10), 1174, DOI: 10.3390/catal12101174.

66 J. Kang, Y. Song, T. Kim and S. Kim, Recent trends in the development of reactor systems for hydrogen production via methanol steam reforming, *Int. J. Hydrogen Energy*, 2022, **47**(6), 3587–3610, DOI: 10.1016/j.ijhydene.2021.11.041.

67 D. R. Palo, R. A. Dagle and J. D. Holladay, Methanol steam reforming for hydrogen production, *Chem. Rev.*, 2007, **107**(10), 3992–4021.

68 A. Iulianelli, P. Ribeirinha, A. Mendes and A. Basile, Methanol steam reforming for hydrogen generation via conventional and membrane reactors: a review, *Renewable Sustainable Energy Rev.*, 2014, **29**, 355–368, DOI: 10.1016/j.rser.2013.08.032.

69 D. Iranshahi, A. Golrokh, E. Pourazadi, S. Saeidi and F. Gallucci, Progress in spherical packed-bed reactors: opportunities for refineries and chemical industries, *Chem. Eng. Process.*, 2018, **132**, 16–24, DOI: 10.1016/j.cep.2018.08.004.

70 G. Leonzio and P. U. Foscolo, Analysis of a 2-D model of a packed bed reactor for methanol production by means of CO_2 hydrogenation, *Int. J. Hydrogen Energy*, 2020, **45**(18), 10648–10663, DOI: 10.1016/j.ijhydene.2020.01.248.

71 M. Hosseini Abbandanak, M. Taghizadeh and N. Fallah, High-purity hydrogen production by sorption-enhanced methanol steam reforming over a combination of Cu–Zn–CeO_2–ZrO_2/MCM-41 catalyst and (Li–Na–K) $NO_3 \cdot MgO$ adsorbent, *Int. J. Hydrogen Energy*, 2021, **46**(10), 7099–7112, DOI: 10.1016/j.ijhydene.2020.11.250.

72 J. Chicano, C. T. Dion, U. Pasaogullari and J. A. Valla, Simulation of 12-bed vacuum pressure-swing adsorption for hydrogen separation from methanol-steam reforming off-gas, *Int. J. Hydrogen Energy*, 2021, **46**(56), 28626–28640, DOI: 10.1016/j.ijhydene.2021.06.102.

73 A. Srivastava, P. Kumar and A. Dhar, Performance enhancement of methanol reforming reactor through finned surfaces and diffused entry for on-board hydrogen generation, *Int. J. Hydrogen Energy*, 2022, **47**(11), 7478–7490, DOI: 10.1016/j.ijhydene.2021.12.084.

74 A. Karim, J. Bravo and A. Datye, Nonisothermality in packed bed reactors for steam reforming of methanol, *Appl. Catal., A*, 2005, **282**(1), 101–109, DOI: **10.1016/j.apcata.2004.12.006**.

75 M. M. N. Khan and S. Jayanti, Minimizing Heat Transfer Resistance in an Integrated Methanol Steam Reformer Designed Using Space-Filling Curves, *Ind. Eng. Chem. Res.*, 2022, **61**(15), 5255–5271.

76 A. Karim, J. Bravo, D. Gorm, T. Conant and A. Datye, Comparison of wall-coated and packed-bed reactors for steam reforming of methanol, *Catal. Today*, 2005, **110**(1–2), 86–91, DOI: **10.1016/j.cattod.2005.09.010**.

77 P. Dokamaingam, S. Assabumrungrat, A. Soottitantawat, I. Sramala and N. Laosiripojana, Modeling of SOFC with indirect internal reforming operation: comparison of conventional packed-bed and catalytic coated-wall internal reformer, *Int. J. Hydrogen Energy*, 2009, **34**(1), 410–421, DOI: **10.1016/j.ijhydene.2008.10.055**.

78 S. Hafeez, E. Aristodemou, G. Manos, S. M. Al-Salem and A. Constantinou, Modelling of packed bed and coated wall microreactors for methanol steam reforming for hydrogen production, *RSC Adv.*, 2020, **10**(68), 41680–41692, DOI: **10.1039/d0ra06834a**.

79 R. Kusumastuti, P. C. Cheng and C.-J. Tseng, A numerical study of internally heating, counter-flow tubular packed bed reactor for methanol steam reforming, *Int. J. Hydrogen Energy*, 2024, **52**, 964–977, DOI: **10.1016/j.ijhydene.2023.04.187**.

80 H. Zhang, *et al.*, Enhancement of methanol steam reforming in a tubular fixed-bed reactor with simultaneous heating inside and outside, *Energy*, 2022, **254**, 124330, DOI: **10.1016/j.energy.2022.124330**.

81 J. Wang, *et al.*, Thermal analysis of a micro tubular reactor for methanol steam reforming by optimizing the multilayer arrangement of catalyst bed for the catalytic combustion of methanolr, *Int. J. Hydrogen Energy*, 2023, **48**(73), 28315–28332, DOI: **10.1016/j.ijhydene.2023.03.450**.

82 J. Zhu, S. S. Araya, X. Cui, S. L. Sahlin and S. K. Kær, Modeling and design of a multi-tubular packed-bed reactor for methanol steam reforming over a Cu/ZnO/Al$_2$O$_3$ catalyst, *Energies*, 2020, **13**(3), 610, DOI: **10.3390/en13030610**.

83 J. Shi, Q. Wu, D. Mei, H. Liu and Y. Wang, Development of pure hydrogen generation system based on methanol steam reforming and Pd membrane, *Int. J. Hydrogen Energy*, 2024, **69**, 147–157, DOI: **10.1016/j.ijhydene.2024.04.359**.

84 C. Wang, *et al.*, Configuration of coupling methanol steam reforming over Cu-based catalyst in a synthetic palladium membrane for one-step high purity hydrogen production, *J. Energy Inst.*, 2023, **108**, 101245, DOI: **10.1016/j.joei.2023.101245**.

85 K. Ghasemzadeh, J. N. Harasi, T. Y. Amiri, A. Basile and A. Iulianelli, Methanol steam reforming for hydrogen generation: a comparative modeling study between silica and Pd-based membrane reactors by CFD method, *Fuel Process. Technol.*, 2020, **199**, 106273, DOI: **10.1016/j.fuproc.2019.106273**.

86 K. Ghasemzadeh, N. Jafar Harasi, A. Iulianelli and A. Basile, Theoretical evaluation of various configurations of silica membrane reactor in methanol steam reforming using CFD method, *Int. J. Hydrogen Energy*, 2020, **45**(12), 7354–7363, DOI: **10.1016/j.ijhydene.2019.05.090**.

87 A. Cifuentes, L. Soler, R. Torres and J. Llorca, Methanol steam reforming over PdZn/ZnAl$_2$O$_4$/Al$_2$O$_3$ in a catalytic membrane reactor: an experimental and modelling study, *Int. J. Hydrogen Energy*, 2022, **47**(22), 11574–11588, DOI: **10.1016/j.ijhydene.2022.01.186**.

88 M. Saidi, Performance assessment and evaluation of catalytic membrane reactor for pure hydrogen production via steam reforming of methanol, *Int. J. Hydrogen Energy*, 2017, **42**(25), 16170–16185, DOI: **10.1016/j.ijhydene.2017.05.130**.

89 S. Liu, P. Du, H. Jia, Q. Zhang and L. Hao, Study on the impact of methanol steam reforming reactor channel structure on hydrogen production performance, *Renewable Energy*, 2024, **228**, 120612, DOI: **10.1016/j.renene.2024.120612**.

90 X. Zhuang, X. Xu, L. Li and D. Deng, Numerical investigation of a multichannel reactor for syngas production by methanol steam reforming at various operating conditions, *Int. J. Hydrogen Energy*, 2020, **45**(29), 14790–14805, DOI: **10.1016/j.ijhydene.2020.03.207**.

91 M. M. Sarafraz, M. R. Safaei, M. Goodarzi and M. Arjomandi, Reforming of methanol with steam in a micro-reactor with Cu–SiO$_2$ porous catalyst, *Int. J. Hydrogen Energy*, 2019, **44**(36), 19628–19639, DOI: **10.1016/j.ijhydene.2019.05.215**.

92 Q. Wu, Y. Wang, D. Mei and S. Si, Development of methanol steam reforming microreactor based on stacked wave sheets and copper foam for hydrogen production, *Int. J. Hydrogen Energy*, 2022, **47**(9), 6282–6294, DOI: **10.1016/j.ijhydene.2021.11.221**.

93 Q. Wu, D. Mei, X. Qiu and Y. Wang, Development of multilevel amplified methanol steam reforming microreactor with high hydrogen production rate, *Fuel*, 2023, **350**, 128800, DOI: **10.1016/j.fuel.2023.128800**.

94 S. Fan, *et al.*, A flow-through catalytic membrane micro-reactor for hydrogen production by methanol steam reforming, *Chem. Eng. Sci.*, 2023, **282**, 119283, DOI: **10.1016/j.ces.2023.119283**.

95 J. Zhu, S. S. Araya, X. Cui and S. K. Kær, The role of effectiveness factor on the modeling of methanol steam reforming over CuO/ZnO/Al$_2$O$_3$ catalyst in a multi-tubular reactor, *Int. J. Hydrogen Energy*, 2022, **47**(14), 8700–8715, DOI: **10.1016/j.ijhydene.2021.12.223**.

96 Y. Choi and H. G. Stenger, Kinetics, simulation and optimization of methanol steam reformer for fuel cell applications, *J. Power Sources*, 2005, **142**(1), 81–91, DOI: **10.1016/j.jpowsour.2004.08.058**.

97 S. S. Rahatade and N. A. Mali, Techno-economic assessment of hydrogen production via dimethylether steam reforming and methanol steam reforming, *Indian Chem. Eng.*, 2023, **65**(4), 352–368, DOI: **10.1080/00194506.2022.2162450**.

98 K. He, C. Zhang, Q. He, Q. Wu, L. Jackson and L. Mao, Effectiveness of PEMFC historical state and operating mode in PEMFC prognosis, *Int. J. Hydrogen Energy*, 2020, **45**(56), 32355–32366, DOI: **10.1016/j.ijhydene.2020.08.149**.

99 T. Y. Amiri, K. Ghasemzageh and A. Iulianelli, Membrane reactors for sustainable hydrogen production through steam reforming of hydrocarbons: a review, *Chem. Eng. Process.*, 2020, **157**, 108148, DOI: **10.1016/j.cep.2020.108148**.

100 A. Iulianelli, P. Ribeirinha, A. Mendes and A. Basile, Methanol steam reforming for hydrogen generation via conventional and membrane reactors: a review, *Renewable Sustainable Energy Rev.*, 2014, **29**, 355–368, DOI: **10.1016/j.rser.2013.08.032**.

101 E. Y. Mironova, *et al.*, Methanol Steam Reforming in a Reactor with a Palladium–Copper Membrane in the Presence of a Nickel–Copper Catalyst, *Pet. Chem.*, 2020, **60**(11), 1232–1238, DOI: **10.1134/S0965544120110158**.

102 O. Jazani, J. Bennett and S. Liguori, Carbon-low, renewable hydrogen production from methanol steam reforming in membrane reactors – a review, *Chem. Eng. Process.*, 2023, **189**, 109382, DOI: **10.1016/j.cep.2023.109382**.

103 M. Byun, B. Lee, H. Lee, S. Jung, H. Ji and H. Lim, Techno-economic and environmental assessment of methanol steam reforming for H$_2$ production at various scales, *Int. J. Hydrogen Energy*, 2020, **45**(46), 24146–24158, DOI: **10.1016/j.ijhydene.2020.06.097**.

104 M. Byun, H. Kim, H. Lee, D. Lim and H. Lim, Conceptual design for methanol steam reforming in serial packed-bed reactors and membrane filters: economic and environmental perspectives, *Energy*, 2022, **241**, 122516, DOI: **10.1016/j.energy.2021.122516**.

105 S. Kim, *et al.*, Steam reforming of methanol for ultra-pure H$_2$ production in a membrane reactor: techno-economic analysis, *Int. J. Hydrogen Energy*, 2019, **44**(4), 2330–2339, DOI: **10.1016/j.ijhydene.2018.08.087**.

106 X. Yao, Y. Zhang, L. Du, J. Liu and J. Yao, Review of the applications of microreactors, *Renewable Sustainable Energy Rev.*, 2015, **47**, 519–539, DOI: **10.1016/j.rser.2015.03.078**.

107 V. Spallina, G. Motamedi, F. Gallucci and M. van Sint Annaland, Techno-economic assessment of an integrated high pressure chemical-looping process with packed-bed reactors in large scale hydrogen and methanol production, *Int. J. Greenhouse Gas Control*, 2019, **88**, 71–84, DOI: **10.1016/j.ijggc.2019.05.026**.

108 H. Ma, M. Zhou, W. Ying and D. Fang, Two-dimensional modeling of a plant-scale fixed-bed reactor for hydrogen production from methanol steam reforming, *Int. J. Hydrogen Energy*, 2016, **41**(38), 16932–16943, DOI: **10.1016/j.ijhydene.2016.07.117**.

109 S. Zhou, *et al.*, Design and performance evaluation of flexible tubular microreactor for methanol steam reforming reaction, *Int. J. Hydrogen Energy*, 2022, **47**(85), 36022–36031, DOI: **10.1016/j.ijhydene.2022.08.194**.

110 Y. Wang, H. Liu, D. Mei, Q. Wu and H. Zhou, A novel thermally autonomous methanol steam reforming microreactor using SiC honeycomb ceramic as catalyst support for hydrogen production, *Int. J. Hydrogen Energy*, 2021, **46**(51), 25878–25892, DOI: **10.1016/j.ijhydene.2021.05.103**.

111 M. Varmazyari, Y. Khani, F. Bahadoran, Z. Shariatinia and S. Soltanali, Hydrogen production employing Cu(BDC) metal–organic framework support in methanol steam reforming process within monolithic micro-reactors, *Int. J. Hydrogen Energy*, 2021, **46**(1), 565–580, DOI: **10.1016/j.ijhydene.2020.09.245**.

112 Q. Wu, Y. Wang, H. Zhou, X. Qiu and D. Mei, Measurement of reaction temperature distribution inside of methanol steam reforming microreactor using infrared thermography, *Appl. Therm. Eng.*, 2024, **238**, 121909, DOI: **10.1016/j.applthermaleng.2023.121909**.

113 T. Zheng, D. Zhou, Y. Zhan and Y. Xu, Integration design optimization of self-thermal methanol steam reforming microreactor for hydrogen production, *Int. J. Hydrogen Energy*, 2023, **48**(84), 32642–32653, DOI: **10.1016/j.ijhydene.2023.05.013**.

114 G. Zhang, J. Zhao, Q. Wang, T. Yang, Q. Zhang and L. Zhang, Fast start-up structured CuFeMg/Al$_2$O$_3$ catalyst applied in microreactor for efficient hydrogen production in methanol steam reforming, *Chem. Eng. J.*, 2021, **426**, 130644, DOI: **10.1016/j.cej.2021.130644**.

115 W. Lu, *et al.*, Microchannel structure design for hydrogen supply from methanol steam reforming, *Chem. Eng. J.*, 2022, **429**, 132286, DOI: **10.1016/j.cej.2021.132286**.

116 J. Chen and Y. Yu, Numerical modelling for design of microchannel reactors: application to hydrogen production from methanol by steam reforming, *Int. J. Hydrogen Energy*, 2024, **50**, 1526–1540, DOI: **10.1016/j.ijhydene.2023.11.061**.

117 X. Zhuang, X. Xia, X. Xu and L. Li, Experimental investigation on hydrogen production by methanol steam reforming in a novel multichannel micro packed bed reformer, *Int. J. Hydrogen Energy*, 2020, **45**(19), 11024–11034, DOI: **10.1016/j.ijhydene.2020.02.034**.

118 A. Kampker, H. Heimes, M. Kehrer, S. Hagedorn, P. Reims and O. Kaul, Fuel cell system production cost modeling and analysis, *Energy Reports*, 2023, **9**, 248–255, DOI: **10.1016/j.egyr.2022.10.364**.

119 Z. Hua, Z. Zheng, E. Pahon, M.-C. Péra and F. Gao, A review on lifetime prediction of proton exchange membrane fuel cells system, *J. Power Sources*, 2022, **529**, 231256, DOI: **10.1016/j.jpowsour.2022.231256**.

120 S. J. Peighambardoust, S. Rowshanzamir and M. Amjadi, Review of the proton exchange membranes for fuel cell applications, *Int. J. Hydrogen Energy*, 2010, **35**(17), 9349–9384, DOI: **10.1016/j.ijhydene.2010.05.017**.

121 N. Li, *et al.*, A review of reformed methanol-high temperature proton exchange membrane fuel cell systems, *Renewable Sustainable Energy Rev.*, 2023, **182**, 113395, DOI: **10.1016/j.rser.2023.113395**.

122 K. Kappis, J. Papavasiliou and G. Avgouropoulos, Methanol Reforming Processes for Fuel Cell Applications, *Energies*, 2021, **14**(24), 8442, DOI: **10.3390/en14248442**.

123 E. Qu, *et al.*, Proton exchange membranes for high temperature proton exchange membrane fuel cells: challenges and perspectives, *J. Power Sources*, 2022, **533**, 231386, DOI: **10.1016/j.jpowsour.2022.231386**.

124 S. Xing, C. Zhao, S. Ban, H. Su, M. Chen and H. Wang, A hybrid fuel cell system integrated with methanol steam reformer and methanation reactor, *Int. J. Hydrogen Energy*, 2021, **46**(2), 2565–2576, DOI: **10.1016/j.ijhydene.2020.10.107**.

125 P. Ribeirinha, G. Schuller, M. Boaventura and A. Mendes, Synergetic integration of a methanol steam reforming cell with a high temperature polymer electrolyte fuel cell, *Int. J. Hydrogen Energy*, 2017, **42**(19), 13902–13912, DOI: **10.1016/j.ijhydene.2017.01.172**.

126 P. Ribeirinha, M. Abdollahzadeh, J. M. Sousa, M. Boaventura and A. Mendes, Modelling of a high-temperature polymer electrolyte membrane fuel cell integrated with a methanol steam reformer cell, *Appl. Energy*, 2017, **202**, 6–19, DOI: **10.1016/j.apenergy.2017.05.120**.

127 P. Ribeirinha, M. Abdollahzadeh, A. Pereira, F. Relvas, M. Boaventura and A. Mendes, High temperature PEM fuel cell integrated with a cellular membrane methanol steam reformer: experimental and modelling, *Appl. Energy*, 2018, **215**, 659–669, DOI: **10.1016/j.apenergy.2018.02.029**.

128 M. Liu, Y. Shi and N. Cai, Modeling of Packed Bed Methanol Steam Reformer Integrated with Tubular High Temperature Proton Exchange Membrane Fuel Cell, *J. Therm. Sci.*, 2023, **32**(1), 81–92, DOI: **10.1007/s11630-022-1764-9**.

129 Z. Chen, B. Yin, Z. Wei and F. Dong, Coupling of high-temperature proton exchange membrane fuel cells with methanol steam reforming: modeling and simulation for an integrated coupled for power generation system, *Energy Convers. Manage.*, 2024, **301**, 118044, DOI: **10.1016/j.enconman.2023.118044**.

130 O. Özcan and A. N. Akın, Methanol steam reforming kinetics using a commercial CuO/ZnO/Al$_2$O$_3$ catalyst: simulation of a reformer integrated with HT-PEMFC system, *Int. J. Hydrogen Energy*, 2023, **48**(60), 22777–22790, DOI: **10.1016/j.ijhydene.2023.01.093**.

131 Y. Li, *et al.*, Performance analysis and optimization of a novel vehicular power system based on HT-PEMFC integrated methanol steam reforming and ORC, *Energy*, 2022, **257**, 124729, DOI: **10.1016/j.energy.2022.124729**.

132 Z. Liang, *et al.*, Integration and optimization of methanol-reforming proton exchange membrane fuel cell system for distributed generation with combined cooling, heating and power, *J. Cleaner Prod.*, 2023, **411**, 137342, DOI: **10.1016/j.jclepro.2023.137342**.